MinPlotX v2.0 – Mineral Calculation and Basic Plotting Routines

Jesse B. Walters, Nils B. Gies

Table of content

Section 1: Introduction

MinPlotX v2.0 is a MATLAB®-based mineral formula recalculation and compositional plotting program for electron microprobe analyses (EPMA). The program offers recalculation and structural formula assignment for 21 different mineral groups: allanite, amphibole, apatite, chlorite, chloritoid, cordierite, epidote, feldspar, garnet, ilmenite, lawsonite, mica, olivine, oxyspinel, pyroxene, scapolite, serpentine, staurolite, sulfides, talc, and titanite. In all cases, the basic formula recalculation is laid out in Walters (2022). All mineral abbreviations follow Warr (2021). Procedures for multivalent elements (Section 2) and mineral specific options (Section 3) are presented here in detail. There is also an 'unknown' option that allows the calculation of mineral apfu for any mineral (see Section 4).

Basic mineral compositional plotting options are also described here (with example plots). These are the plots which are automatically generated for each mineral by clicking *Quickplot* or *Easy Plot* in the GUI. Plots are typically those commonly used for the given mineral and are selected based on community standards. MinPlotX offers significant flexibility for the user to create nearly any other mineral compositional plots using the visualization module (*VisModule*), advanced plot module (*AdvancedPlotModule*), spot visualization module for spatially referenced data (*SpotVis*), or chemical correlation diagrams (*GeoCPlot*). These modules are found under the *Results* tab.

Section 1.1: Types of input data for MinPlotX

MinPlotX reads tables of mass percent of the oxides of the elements (for silicate, oxide, and phosphate minerals) or mass percent of elements (for sulfides only). Some oxides are required for minerals (*e.g.*, SiO_2 in silicates) whereas others are optional (*e.g.*, SrO in feldspar, K_2O in pyroxene). All possible inputs (required and optional), calculated outputs, and mineral specific options are given in *MinPlotX_InputsOutputs.xlsx*. This document should be checked in detail before loading any data into MinPlotX.

Data files can include either a single mineral (*e.g.*, only olivine) or multiple minerals with a metadata column of mineral names assigned to each analysis. For single minerals, if the input file is named after the mineral, then MinPlotX will automatically assign the correct calculation for the loaded data file. Otherwise, the *unknown* (generic procedure) is automatically assigned and user must select the appropriate calculation scheme using the *mineral* dropdown menu. If multiple minerals are included in a single datafile, then the user must go to the *MultiMineralCalc* tab to proceed with mineral formula recalculation. The *MultiMineralCalc* tab offers the same functionality as mineral formula recalculation under the Main tab, with mineral specific options, such as *Fe3_ratio*, *tetra_Fe3*, and others, depending on the minerals selected.

Section 2: Options for multi-valent elements

MinPlotX has multiple ways to handle elements that are multi-valent to provide maximum flexibility. Options are available for Fe^{3+} and Fe^{2+} for most minerals (*Fe Options* window in MinPlotX) and Mn^{3+} and Mn^{2+} is considered for some minerals (*Mn Options* window in MinPlotX). If the Fe Options or Mn Options window is not present for a certain mineral then a default valence state is only possible for that mineral and corresponding element (*e.g.*, $\Sigma Fe = Fe^{2+}$ only in feldspar, $\Sigma Fe = Fe^{3+}$ only in titanite). In all cases, any combination of Fe_2O_3, FeO, Mn_2O_3 and MnO are possible inputs for all phases with these elements. Multivalent options are also available for sulfur in apatite (see Section 3.3).

Section 2.1: Options for Fe^{3+} and Fe^{2+}

To consider Fe^{3+} in the formula recalculation the *Calculate with Fe^{3+}* box must be checked. Depending on the mineral, multiple options are available for Fe^{3+} and Fe^{2+}. The simplest option is using the $Fe^{3+}/\Sigma Fe$ corresponding to the data in the input file. This is achieved by selecting the *Use Fe3/FeTotal Ratio (From Table)* check box. The user can input measured (or estimated) Fe_2O_3 and FeO, ΣFeO and a column of $Fe^{3+}/\Sigma Fe$ ratios (given as *Fe3_ratio* in the input data file), or ΣFe_2O_3 and a column of $Fe^{3+}/\Sigma Fe$ ratios. Any combination of these will result in calculated Fe^{3+} and Fe^{2+} in the final apfu and structural formula outputs.

Alternatively, the user can use a global $Fe^{3+}/\Sigma Fe$ ratio can be assigned to all analyses by selecting the *Use Global Fe3/FeTotal* Ratio check box. This option activates a space in the Fe Options window to enter a ratio (between 0 and 1).

Stoichiometric estimation of $Fe^{3+}/\Sigma Fe$ is available for amphibole, chloritoid, garnet, ilmenite, pyroxene, and spinel. The procedure is mineral specific and is detailed in Section 3.

Finally, it is possible to give the fraction of Fe^{3+} on the tetrahedral site ($^{IV}Fe^{3+}/\Sigma Fe^{3+}$) for chlorite, mica, serpentine, and talc. The fraction of tetrahedral Fe^{3+} can be read as *tetra_Fe3* if it is given as a data column in the input data file. It is also possible to specify a global value for all analyses. If no global value is given and *tetra_Fe3* is not in the input file, then the default $^{IV}Fe^{3+}/\Sigma Fe^{3+} = 0$ is assumed.

If no Fe^{3+} options are checked or *Calculate with Fe3+* is not available for a given mineral then $\Sigma Fe = Fe^{2+}$, with the exception of titanite where ΣFe is always assumed to be Fe^{3+}.

Section 2.2: Options for Mn^{3+} and Mn^{2+}

To consider Mn^{3+} in the formula recalculation the *Calculate with Mn3+* box must be checked. Calculation of Mn^{3+} and Mn^{2+} is possible for allanite, epidote, ilmenite, and lawsonite. Calculation is possible by giving a measured (or estimated) Mn^{3+} and Mn^{2+} in the input datafile read by MinPlotX as Mn_2O_3 and MnO, ΣMnO and a column of $Mn^{3+}/\Sigma Mn$ ratios (given as *Mn3_ratio* in the input data file), or ΣMn_2O_3 and a column of $Mn^{3+}/\Sigma Mn$ ratios. Alternatively, a global $Mn^{3+}/\Sigma Mn$ ratios can be specified. If no Mn^{3+} options are checked or *Calculate with Mn3+* is not available for a given mineral, then ΣMn is always equal to Mn^{2+}.

Stoichiometric estimation of Fe^{3+} assumes that Fe is the only multivalent element in the mineral under consideration. Generally, this estimate is calculated by difference between the oxygens calculated from cation normalization and the ideal number of oxygens, as a result it cannot be known how much of this difference is assigned to multivalent Fe or multivalent Mn. Most minerals and rocks are Mn-poor and as a result ignoring Mn^{3+} for Mn-poor minerals is a better approximation than assuming Fe^{3+} is equal to zero. Additionally, the transition from MnO to Mn_2O_3 occurs at a much higher oxygen fugacity compared to the transition from FeO to Fe_2O_3, thus most rocks are simply not ‘oxidized’ enough for significant Mn^{3+} to exist.

Section 3: Comprehensive description of the mineral formula calculation routines

(in alphabetical order)

Section 3.1: Allanite (and other REE-epidote group minerals)

The allanite mineral formula recalculation function considers a chemical formula of $A_2M_3T_3(O,OH,F)_{13}$ and is an extension of the calculation procedure used for epidote. In the case of allanite and other REE-epidote group minerals, A = Y, REE, Pb, U, Th, K, Na, Sr, Ca, Mg, Mn^{2+}, and Fe^{2+}, M = Mg, Mn^{2+}, Fe^{2+}, Mn^{3+}, Fe^{3+}, Cr, Ti, and ^{IV}Al, and T = ^{IV}Al, Zr, P, and Si. **Table 3.1.1** gives the cation assignment used by the allanite MinPlotX function for selected epidote group endmembers.

Normalization is based on the hydrous basis of 13 oxygen equivalents (12O + OH). If H_2O is not measured, the hydroxyl component is calculated as OH = 1 – (F + Cl) following an iterative normalization scheme. The normalization and OH calculation is then iterated 50 times, far more than necessary for a stable calculated OH content. For analyses without H_2O, F, or Cl

Table 3.1.1 Example structural formula assignments for allanite

Endmember	T	M	A
(Clino-)Zoisite (czo/zo)	Si,Si,Si	Al,Al,Al	Ca,Ca
Epidote (ep)	Si,Si,Si	Al,Al,Fe^{3+}	Ca,Ca
Piemontite (pmt)	Si,Si,Si	Al,Al,Mn^{3+}	Ca,Ca
"Cr-Epidote (Cr-ep)"	Si,Si,Si	Al,Al,Cr	Ca,Ca
allanite (aln)	Si,Si,Si	Al,Al,Fe^{2+}	Ca, (REE, Y, Th, U)
ferriallanite (Fe-aln)	Si,Si,Si	Al,Fe^{3+},Fe^{2+}	Ca, (REE, Y, Th, U)

To prevent an overly long output, the structural formula is reported with a total REE+Y; however, the apfu output gives the content of each individual REE and Y cation. Magnesium, Mn^{2+}, and $Fe^{2+}$are equipartitioned such that X_{Mg} ($Mg/(Mg + Mn^{2+} + Fe^{2+})$), X_{Mn} ($Mn^{2+}/(Mg + Mn^{2+} + Fe^{2+})$), and X_{Fe} ($Fe^{2+}/(Mg + Mn^{2+} + Fe^{2+})$) ratios are equal for M and A cations. Note that chromian epidote is presented as a fictitious endmember accounting for the exchange vector of Cr^{3+} for Fe^{3+}.

3.1.1 Fe-Mn valence options – The substitution of trivalent A-cations in allanite requires charge balance by substitution of divalent Mg, Mn, and Fe M-cations. Therefore, while the assumption that $Fe^{3+}/\Sigma Fe = 1$ and $Mn^{3+}/\Sigma Mn = 1$ is broadly valid for REE-poor epidote group minerals, these assumptions are clearly incorrect for REE-enriched epidote group minerals like allanite or androsite. Ferric Fe and Mn^{3+} can be calculated from ratios (input file or global) or from weight percent FeO, Fe_2O_3, MnO, and Mn_2O_3 values in the input file (see Section 2).

3.1.2 Plotting – Allanite and related REE-epidote group minerals can be plotted in the ΣREE + Y + Th + U vs ^{IV}Al diagram (Fig. 3.1). Strontium is sometimes also included on the Y axis of such plots but is not included here. The reason for excluding Sr is that it is a divalent cation and does not follow the same substitution mechanisms as allanite ($REE^{3+} + M^{2+} = Ca + Al$) and ferriallanite ($REE^{3+} + M^{2+} = Ca + Fe^{3+}$). Including Sr would result in non-allanite group endmembers plotting as allanite, such as Epidote-Sr: $(CaSr)Al_2Fe^{3+}Si_3O_{11}O(OH)$.

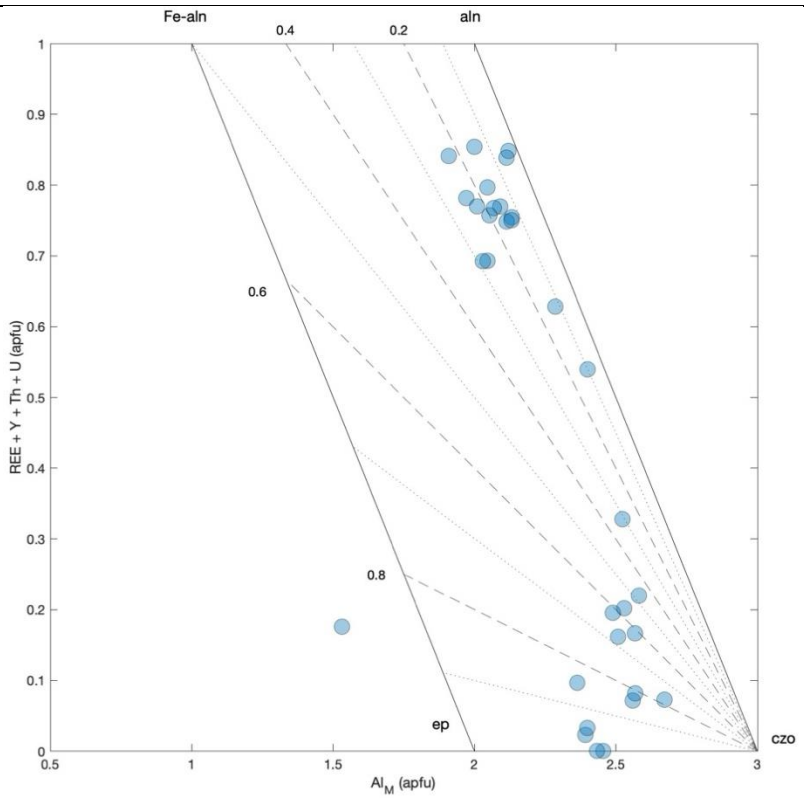

Figure 3.1.1 Plot of ΣREE + Y + Th + U vs ^{IV}Al with isolines of $Fe^{3+}/\Sigma Fe$. Data are from Stumpf *et al.* (2024).

Section 3.2: Amphibole

Amphibole ($AB_2C_5T_8O_{22}W_2$) has a complex structure with a wide compositional space. MinPlotX follows the recommendations of Leake *et al.* (1997) and Hawthorne *et al.* (2012) for structural assignment, with A = □, K, Na, and Ca at the *A* site, B = Ca, Na, Mn, Fe^{2+}, and Mg at the *M*4 site, C = Mn, Fe^{2+}, Mg, Fe^{3+}, Cr, Ti, and Al at the *M*1, *M*3, and *M*2 sites, T = Si and Ti at the *T* site, and OH^-, F^-, Cl^-, and O^{2-} at the *W* site. Minor elements, such as Pb, Zn, Co, V, Sc, and Zr, typically have contents at or below the EPMA detection limit and are not included. Additionally, Li and Be are not routinely measured by EPMA and are also excluded. For a more complete formula recalculation and classification of amphiboles, including Li and other minor elements, see Locock (2014). Tables 3.2.1-3.2.3 give the cation assignments for selected endmembers.

Table 3.2.1 Example structural formula assignments for Na-amphibole

Endmember	W	T	C	B	A
Glaucophane (gln)	OH,OH	Si,Si,Si,Si,Si,Si,Si,Si	Al,Al,Mg,Mg,Mg	Na,Na	
Ferro-glaucophane (Fe-gln)	OH,OH	Si,Si,Si,Si,Si,Si,Si,Si	Al,Al,Fe^{2+},Fe^{2+},Fe^{2+}	Na,Na	
Riebeckite (rbk)	OH,OH	Si,Si,Si,Si,Si,Si,Si,Si	Fe^{3+},Fe^{3+},Fe^{2+},Fe^{2+},Fe^{2+}	Na,Na	
Magnesio-riebeckite (Mg.-rbk)	OH,OH	Si,Si,Si,Si,Si,Si,Si,Si	Fe^{3+},Fe^{3+},Mg,Mg,Mg	Na,Na	
Eckermannite (eck)	OH,OH	Si,Si,Si,Si,Si,Si,Si,Si	Al, Mg,Mg,Mg,Mg	Na,Na	Na
Nybøite (nyb)	OH,OH	Si,Si,Si,Si,Si,Si,Si,Al	Al,Al,Mg,Mg,Mg	Na,Na	Na

Table 3.2.2 Example structural formula assignments for NaCa-amphibole

Endmember	W	T	C	B	A
Barroisite (brs)	OH,OH	Si,Si,Si,Si,Si,Si,Si,Al	Al,Al,Mg,Mg,Mg	Na,Ca	
Taramite (trm)	OH,OH	Si,Si,Si,Si,Si,Si,Al,Al	Al,Al,Mg,Mg,Mg	Na,Ca	Na
Kataphorite (ktp)	OH,OH	Si,Si,Si,Si,Si,Si,Si,Al	Al,Mg,Mg,Mg,Mg	Na,Ca	Na
Winchite (wnc)	OH,OH	Si,Si,Si,Si,Si,Si,Si,Si	Al,Mg,Mg,Mg,Mg	Na,Ca	
Richterite (rct)	OH,OH	Si,Si,Si,Si,Si,Si,Si,Si	Mg,Mg,Mg,Mg,Mg	Na,Ca	Na

Water is handled in three ways. First, if H_2O is included as an input column and the value is > 0 wt. %, then OH is calculated using the known value. Second, amphibole is normalized on the basis of 24(O,OH,F,Cl) where occupancy of the *W*-site is $^W(OH,F,Cl) = 2$ apfu, therefore if H_2O is not analyzed the normalization is based on 23 oxygen equivalents (anhydrous basis) and OH is 2-(F+Cl). Third, if *TiOH_correction* if selected under *MineralSpecificOption*s then the estimated OH content may be corrected from the measured Ti content. Substitution of Ti in the *M*1 site is commonly balanced by incorporation of O^{2-} (Oberti *et al*., 1992):

(3.2.1) $^C R^{2+} + 2^W(OH)^- \rightarrow {}^C Ti^{4+} + 2^W O^{2-}$

As a result, ^{W}(OH,F,Cl) can be calculated as (2 - 2Ti) apfu, thus correcting for the maximum possible contribution of O^{2-} at the *W*-site (Hawthorne *et al*., 2012). This assumes that Ti_{M3} and Ti_{M2} are negligible, which is not always the case (see Tiepolo *et al*., 1999). For the Ti-O^{2-} correction, the normalization factor is >23 oxygen equivalents and adjusted using the Ti content based on Equation 3.2.1.

Table 3.2.3 Example structural formula assignments for Ca-amphibole

Endmember	W	T	C	B	A
Tremolite (tr)	OH,OH	Si,Si,Si,Si,Si,Si,Si,Si	Mg,Mg,Mg,Mg,Mg	Ca,Ca	
Ferro-actinolite (Fe-act)	OH,OH	Si,Si,Si,Si,Si,Si,Si,Si	Fe^{2+},Fe^{2+},Fe^{2+},Fe^{2+},Fe^{2+}	Ca,Ca	
Magnesio-hornblende (Mg-hbl)	OH,OH	Si,Si,Si,Si,Si,Si,Si,Al	Al,Mg,Mg,Mg,Mg	Ca,Ca	
Ferro-hornblende (Fe-hbl)	OH,OH	Si,Si,Si,Si,Si,Si,Si,Al	Al,Fe^{2+},Fe^{2+},Fe^{2+},Fe^{2+}	Ca,Ca	
Tschermakite (tsr)	OH,OH	Si,Si,Si,Si,Si,Si,Al,Al	Al,Al,Mg,Mg,Mg	Ca,Ca	
Ferro-Tschermakite (Fe-tsr)	OH,OH	Si,Si,Si,Si,Si,Si,Al,Al	Al,Al,Fe^{2+},Fe^{2+},Fe^{2+}	Ca,Ca	
Sadanagaite (sdg)	OH,OH	Si,Si,Si,Si,Si,Al,Al,Al	Al,Al,Mg,Mg,Mg	Ca,Ca	Na
Pargasite (prg)	OH,OH	Si,Si,Si,Si,Si,Si,Al,Al	Al,Mg,Mg,Mg,Mg	Ca,Ca	Na
Edenite (ed)	OH,OH	Si,Si,Si,Si,Si,Si,Si,Al	Mg,Mg,Mg,Mg,Mg	Ca,Ca	Na

3.2.1 Fe-Mn valence options – Amphibole can be calculated in multiple ways. Estimation of Fe^{3+} and Fe^{2+} by charge balance, prescribing Fe^{3+} and Fe^{2+} in the input data (either as FeO and Fe_2O_3 or by including a column labeled *Fe3_ratio*), by assigning a global $Fe^{3+}/\Sigma Fe$ ratio, or by not selecting Fe^{3+} as an option the amphibole formula will be calculated as $\Sigma Fe = Fe^{2+}$. In all cases $\Sigma Mn = Mn^{2+}$. If the user choses to use a prescribed Fe^{3+} and Fe^{2+}, a global value, or $\Sigma Fe = Fe^{2+}$, then the oxygen-based normalization is used (which is adjusted if *TiOH_correction* enabled, see above).

For ferric iron estimation, it can be calculated through normalization to sets of cation sums which provide lower and upper $Fe^{3+}/\Sigma Fe$ limits (Leake *et al.*, 1997; Hawthorne *et al*., 2012). It is important to note that stoichiometric estimation of Fe^{3+}-Fe^{2+} requires all major cations to be analyzed and is thus not appropriate here for Li-rich compositions. Additionally, Fe^{3+} may couple to dehydrogenation, which is not considered in MinPlotX. The Fe^{3+}-Fe^{2+} calculation procedure is as follows. First, the all-ferrous formula is calculated to give the maximum number of cations. Lower $Fe^{3+}/\Sigma Fe$ limits are calculated from the all-ferrous formula based on the three following criteria:

(1-1) Si ≤8 apfu

(1-2) $(Si + Al + Ti + Cr + Fe^{2+} + Fe^{3+} + Mn + Mg + Ca + Na + K) \leq 16$ apfu

(1-3) $(Si + Al + Ti + Cr + Fe^{2+} + Fe^{3+} + Mn + Mg + Ca) \leq 15$ apfu

Criteria 1-1 and 1-2 are set by the structure. There cannot be more than 8 Si cations on the *T* site or 16 total cations. Criterion 1-3 assumes that Ca does not incorporate into the *A*-site, which may not be true in amphiboles from Ca-rich rocks, like marbles and calc-silicates (Hawthorne *et al*., 2012). If none of these criteria are invalidated, the minimum Fe^{3+} estimate comes from the all-ferrous formula. The upper $Fe^{3+}/\Sigma Fe$ limits are calculated using the five following criteria:

(2-1) $(Si + Al) = 8$ apfu

(2-2) $(Si + Al + Ti + Cr + Fe^{2+} + Fe^{3+} + Mn + Mg + Ca + Na) = 15$ apfu

(2-3) $(Si + Al + Ti + Cr + Fe^{2+} + Fe^{3+} + Mn + Mg) = 13$ apfu

(2-4) (Si + Al + Ti + Cr + Fe^{3+}) = 10 apfu

(2-5) $\Sigma Fe=Fe^{3+}$

Criterion 2-1 assumes that Si and Al only substitute at the tetrahedral site; whereas, criterion 2-2 assumes that only K substitutes at the *A* site. Hawthorne *et al*. (2012) warn that criteria 2-1 and 2-2 are not appropriate for high-temperature richterite compositions where Ti may occur as a T cation and K may occur as a B cation. It is important to note that the estimation schemes here will not explicitly yield the Ti and K occupancies needed to identify this composition, and caution must be taken if this composition is suspected. Additionally, criterion 2-2 is inappropriate for amphiboles with an edenite ($NaCa_2Mg_5(Si_7Al)O_{22}(OH)_2$) component, such as hornblende, as it assumes Na is not an A cation. Criterion 2-3 assumes that C = Fe^{2+}, Mn, or Mg, which may be violated if these elements also substitute for B group cations. Criterion 2-4 assumes that 3+ and 4+ cations fill the *T* and *M*2 sites, and the normalization factor is calculated as 36/(46-Si-Ti-Al-Cr) (Leake *et al.*, 1997). Finally, an all-ferric formula provides the extreme upper $Fe^{3+}/\Sigma Fe$ limit.

MinPlotX automatically selects the appropriate lower and upper Fe^{3+} limits. Only one minimum and maximum choice is possible for each analysis. The lower limit is selected as the criterion which gives the minimum normalization factor; however, if all the normalization factors have values greater one, then the $\Sigma Fe=Fe^{2+}$ formula provides the lower limit. Additionally, if the three minima criteria have normalization factors which are lower than those for the four maximum criteria, then Fe^{3+} cannot be estimated and the $\Sigma Fe=Fe^{2+}$ formula is output. In contrast, the maximum normalization factor provides the best estimate for the upper $Fe^{3+}/\Sigma Fe$ limit. After the upper and lower limits are chosen, MinPlotX calculates the mean composition between these limits (Leake *et al*., 1997; Hawthorne *et al*., 2012).

3.2.2 Plotting – Amphibole analyses are automatically assigned to plots for Ca ($^{B}Ca/^{B}(Ca+Na) \geq 0.75$), Na-Ca ($0.75 > {}^{B}Ca/^{B}(Ca+Na) > 0.25$), and Na ($^{B}Ca/^{B}(Ca+Na) \leq 0.25$) groups. The classification scheme of Hawthorne *et al.* (2012) is used: Amphibole compositions are plotted as $^{C}(Al + Fe^{3+} + 2Ti)$ on the x-axis and $^{A}(Na + K + 2Ca)$ on the y-axis (Figs. 4A, 4C). There are two problems with this classification, 1. It is very sensitive to the estimated Fe^{3+} content and 2. The compositional space of some common endmember species are not explored (e.g., classification of amphibole as actinolite and riebeckite is not possible). For these reasons, MinPlotX includes Si (apfu) vs. X_{Mg} and $Fe^{3+}/(Al + Fe^{3+} + Ti)$ vs. $Fe^{2+}/(Fe^{2+} + Mg + Mn)$ classification plots for Ca-amphiboles and Na-amphiboles, respectively (Fig. 4B and D). Additionally, a plot of ΣFe (apfu) vs $Fe^{3+}/\Sigma Fe$ is available, which can be useful for tracking changes in Fe^{3+} content with overall changes in Fe content. Currently plotting options for orthoamphibole are not available.

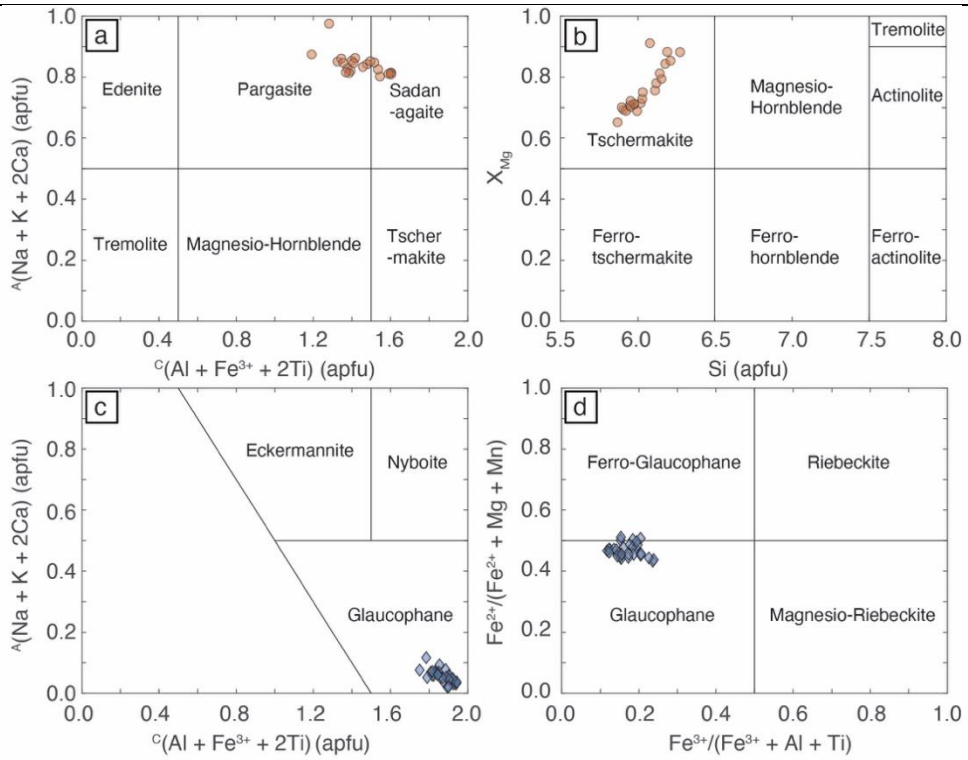

Figure 3.2.1 Clinoamphibole compositional and classification diagrams (after Hawthorne et al., 2012; Leake *et al*., 1997): (A) $^{C}(Al + Fe^{3+} + 2Ti)$ vs $^{A}(Na + K + 2Ca)$ diagram for Ca-amphibole, (B) Si vs X_{Mg} diagram for Ca-Amphibole, (C) $^{C}(Al + Fe^{3+} + 2Ti)$ vs $^{A}(Na + K + 2Ca)$ diagram for Na-amphibole, and (D) $Fe^{3+}/(Fe^{3+} + Al + Ti)$ vs $Fe^{2+}/(Fe^{2+} + Mg + Mn)$ diagram for Na-amphibole. Analyses of glaucophane are collected on blueschists from Port Macquarie, Australia (PMQ065). Ca-amphibole analyses are collected on zoned amphibole from a retrogressed eclogite from Svetlik-Sus, Czech Republic (SVS-11-01; Walters *et al*., 2019; 2021). Figure and caption from Walters *et al.* (2022).

Section 3.3: Apatite

Apatite ($M_{10}(TO_4)_6Z_2$) is calculated in MinPlotX as M = La, Ce, Na, K, Sr, Ba, Ca, Mg, Mn, Fe^{2+}, Al, and Ti, T = P, Si, C^{4+}, S^{4+}, and S^{6+}, and Z = OH, F, Cl, C^{4+}, S^{1-}, and S^{2-} (See Table 3.3.1). If H_2O is not measured, formula recalculation uses an anhydrous normalization to 25 oxygen equivalents (excluding S^{1-}, S^{2-}, F, and Cl) following Ketcham (2015). This method produced the correct results for synthetic apatite compositions when including S^{2-}, whereas normalization on 26 oxygen equivalents - 0.5(F + Cl + S^{1-}) - S^{2-} did not produce accurate results. In this case, there is no iteration to determine OH contents, which are simply calculated as 2 - (F + Cl + S^{1-} + 2 * S^{2-}). If H_2O is measured, then normalization to 26 oxygen equivalents is used.

Since the OH content is calculated by 2 - (F + Cl + C^{4+} + S^{1-} + 2 * S^{2-}) it is possible to calculate negative OH contents if (F + Cl + C^{4+} + S^{1-} + 2 * S^{2-}) > 2 as the Z anions are not normalized before plotting. This is intentional: Fluorine migration and loss is easily induced by the electron beam during EPMA analysis of apatite resulting in F contents that exceed stoichiometric limits (*e.g.*, Goldoff *et al*., 2012). Negative OH contents and F > 2 apfu are an important monitor of beam damage and F migration and therefore no upper limit is placed on F or lower limit on OH in MinPlotX.

Table 3.3.1 Example structural formula assignments for apatite

End-member	Z	T	M
hydroxylapatite	OH^-, OH^-	P,P,P,P,P,P	Ca,Ca,Ca,Ca,Ca,Ca,Ca,Ca,Ca,Ca
chloroapatite	Cl^-, Cl^-	P,P,P,P,P,P	Ca,Ca,Ca,Ca,Ca,Ca,Ca,Ca,Ca,Ca
fluoroapatite	F^-, F^-	P,P,P,P,P,P	Ca,Ca,Ca,Ca,Ca,Ca,Ca,Ca,Ca,Ca
alforsite	Cl^-, Cl^-	P,P,P,P,P,P	Ba,Ba,Ba,Ba,Ba,Ba,Ba,Ba,Ba,Ba
pieczkaite	Cl^-, Cl^-	P,P,P,P,P,P	Mn^{2+},Mn^{2+},Mn^{2+},Mn^{2+},Mn^{2+},Mn^{2+},Mn^{2+},Mn^{2+},Mn^{2+},Mn^{2+}
stronadelphite	F^-, F^-	P,P,P,P,P,P	Sr,Sr,Sr,Sr,Sr,Sr,Sr,Sr,Sr,Sr
britholite-(Ce)	OH^-, OH^-	Si,Si,Si,Si,Si,Si	Ca,Ca,Ca,Ca,Ce,Ce,Ce,Ce,Ce,Ce
britholite-(La)	OH^-, OH^-	Si,Si,Si,Si,Si,Si	Ca,Ca,Ca,Ca,La,La,La,La,La,La

3.3.1 Sulfur valence options – Assignment of sulfur species follows Sadove *et al*. (2019), which is read by MinPlotX if *Sulfur_species* is checked in the *MineralSpecificOptions* window. If the sulfur speciation is not specified and sulfur is included in the input dataset, then sulfur will be calculated as S^{6+} (sulfate is likely the most common species in S-rich apatite). To assign sulfur species the user must give global values in the table for $S^{6+}/\Sigma S$ (*S6_ratio*), $S^{4+}/\Sigma S$ (*S4_ratio*), $S^{1-}/\Sigma S$ (*S1minus_ratio*), and $S^{2-}/\Sigma S$ (*S2minus_ratio*).

3.3.2 Carbon options – Carbon can substitute as CO_3^{2-} in the T site for P or in the Z site for OH, Cl, F (e.g., Hammerli *et al*., 2021; Fleet *et al*., 2004). We follow the method of Hammerli *et al.* (2021) by modifying the procedure of Ketcham (2015) for CO_3^{2-} substitution where H_2O is not also specified in the input file. The user may specify the fraction of CO_3^{2-} on the Z site (Z_ratio), where the remaining CO_3^{2-} is assigned to the P site. For example, a value of 0 would assign all CO_3^{2-} to the T site.

3.3.3 Fe-Mn valence options – The apatite calculation scheme uses $\Sigma Fe = Fe^{2+}$ and $\Sigma Mn = Mn^{2+}$.

3.3.4 Plotting options – Apatite data can be plotted in the Cl, F, OH ternary (Figure 3.3.1). If sulfur and/or carbon is measured then C, S, and OH are combined, this approximation is reasonable since sulfur is a minor species such that $Cl >> C^{4+} + S^{1-} + S^{2-}$ and $F >> C^{4+} + S^{1-} + S^{2-}$. Beam damage (see above) can result in analyses that plot outside of the Cl, F, OH ternary, thus analyses plotting outside of the ternary are allowed as an important monitor of data quality.

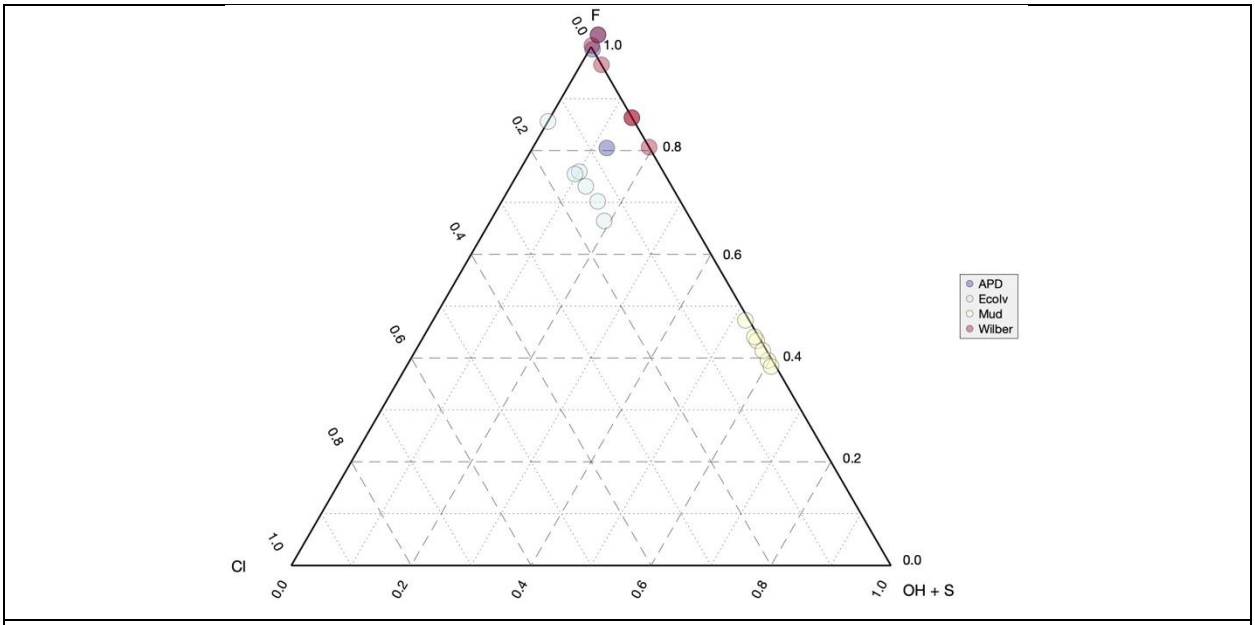

Figure 3.3.1 Cl, F, OH ternary for apatite. Plotted are test data for Durango (APD), Mudtank (Mud), Wilberforce (Wilber), and Eagle Co. (Ecolv) apatite secondary reference materials (as given in Table 3.3.1). Notice that some of the F contents are slightly above one for Wilberforce and Durango, likely due to beam damage during repeated analysis of the secondary reference materials.

Section 3.4: Chlorite

Chlorite ($M_6T_4O_{10}(OH)_8$) is structural formulae are calculated as assigned as M = Mg, Mn^{2+}, Fe^{2+}, Ni, Cr, Ti, $^{VI}Fe^{3+}$, ^{VI}Al, and □ at the octahedral site, whereas T = ^{IV}Al, $^{IV}Fe^{3+}$, and Si at the tetrahedral site (Table 3.4.1). Vacancies on M1 are calculated by □ = $0.5(^{VI}Al - ^{IV}Al) + 0.5^{VI}Fe^{3+}$ following Lanari et al. (2014). If H_2O is measured a hydrous normalization to 18 oxygen equivalents is used, otherwise an anhydrous normalization to 14 oxygen equivalents is used.

3.4.1 Fe-Mn valence options – In low-Fe chlorite, Fe^{3+} substitution may be dominantly the result of exchange with Al, resulting in a fictive 'Fe^{3+}-rich Mg-amesite' endmember (Masci *et al*., 2019). Second, the exchange vector $^{VI}□ + 2^{VI}R^{3+} = 3^{VI}(Mg,Fe^{2+})$ may induce vacancies where R^{3+} is Al or Fe^{3+}. Masci *et al.* (2019) show that a third substitution, following the exchange vector (Fe^{2+}, Mg) + H^+ = Fe^{3+}, may be the primary mechanism behind elevated Fe^{3+} in Fe-rich chlorite. It is possible that other elements, such as Al or Cr, may also substitute via deprotonation. As a result, fully quantitative structural assignment and endmember determination requires the direct analysis of Fe^{3+} and H_2O.

The structural complexities of chlorite preclude Fe^{3+} estimation by charge balance (Schumacher, 1991). Instead, Fe^{3+} and Fe^{2+} can be included in the input data (either as FeO and Fe_2O_3 or by including a column labeled *Fe3_ratio*) or assigned a global $Fe^{3+}/\Sigma Fe$ ratio. If the Fe^{3+} option is not selected, then the chlorite formula will be calculated as $\Sigma Fe = Fe^{2+}$. Additionally, it is possible to give the fraction of Fe^{3+} on the tetrahedral site ($^{IV}Fe^{3+}/\Sigma Fe^{3+}$). The fraction of tetrahedral Fe^{3+} can be read as *tetra_Fe3* from the input file or a global value can be prescribed for all analyses (see Section 2). If no global value is given and *tetra_Fe3* is not in the input file, then the default $^{IV}Fe^{3+}/\Sigma Fe^{3+} = 0$ is assumed.

For manganese, $\Sigma Mn = Mn^{2+}$.

Table 3.4.1 Example structural formula assignments for chlorite

End-member	T	M	Cation Sum	X_{Mg}
chamosite (chm)	Si,Si,Si,Al	Al,Fe^{2+},Fe^{2+},Fe^{2+},Fe^{2+},Fe^{2+}	14	0
clinochlore (cln)	Si,Si,Si,Al	Al,Mg,Mg,Mg,Mg,Mg	14	1
pennanite (pnn)	Si,Si,Si,Al	Al,Mn^{2+},Mn^{2+},Mn^{2+},Mn^{2+},Mn^{2+}	14	0
nimite (nim)	Si,Si,Si,Al	Al,Ni,Ni,Ni,Ni,Ni	14	0
"ferrosudoite (Fe-sud)"	Si,Si,Si,Al	Al,Al,Al,Fe^{2+},Fe^{2+},vac	13	0
sudoite (sud)	Si,Si,Si,Al	Al,Al,Al,Mg,Mg, vac	13	1
"ferrisudoite (Fe^{3+}-sud)"	Si,Si,Si,Al	Fe^{3+},Fe^{3+},Fe^{3+},Mg,Mg,vac	13	1
gonyerite (gye)	Si,Si,Si,Fe^{3+}	Fe^{3+},Mg,Mg,Mg,Mg,Mg	14	1

3.4.2 Plotting – MinPlotX automatically produces four compositional diagrams for chlorite. First, there are two diagrams which plot X_{Mg} vs $^{VI}R^{3+}$. A simplified diagram (Fig. 3.4.1a) after Bailey (1988) which includes only the compositional space between clinochlore

($Mg_5Al(AlSi_3O_{10})(OH)_8$), chamosite ($Fe^{2+}{}_5Al(AlSi_3O_{10})(OH)_8$), sudoite ($Mg_2Al_3(AlSi_3O_{10})(OH)_8$), and a theoretical ferrosudoite endmember ($Fe_2Al_3(AlSi_3O_{10})(OH)_8$). A second diagram (Fig. 3.4.1b) expands this compositional range and subdivides between trioctahedral, di-trioctahedral, and dioctahedral chlorite group minerals. A third diagram plots Si (apfu) vs R^{2+} (apfu) after Wiewiora and Weiss (1990) and is contoured for Al and ^{VI}R (Fig. 3.4.1c). Finally, the diagram of Hey (1954) of Fe_{total} (apfu) vs Si (apfu) is given (Fig. 3.4.1d). The historical names of chlorite subdivisions are retained but are discredited and may be used to visualize compositional trends but should not be used for classification.

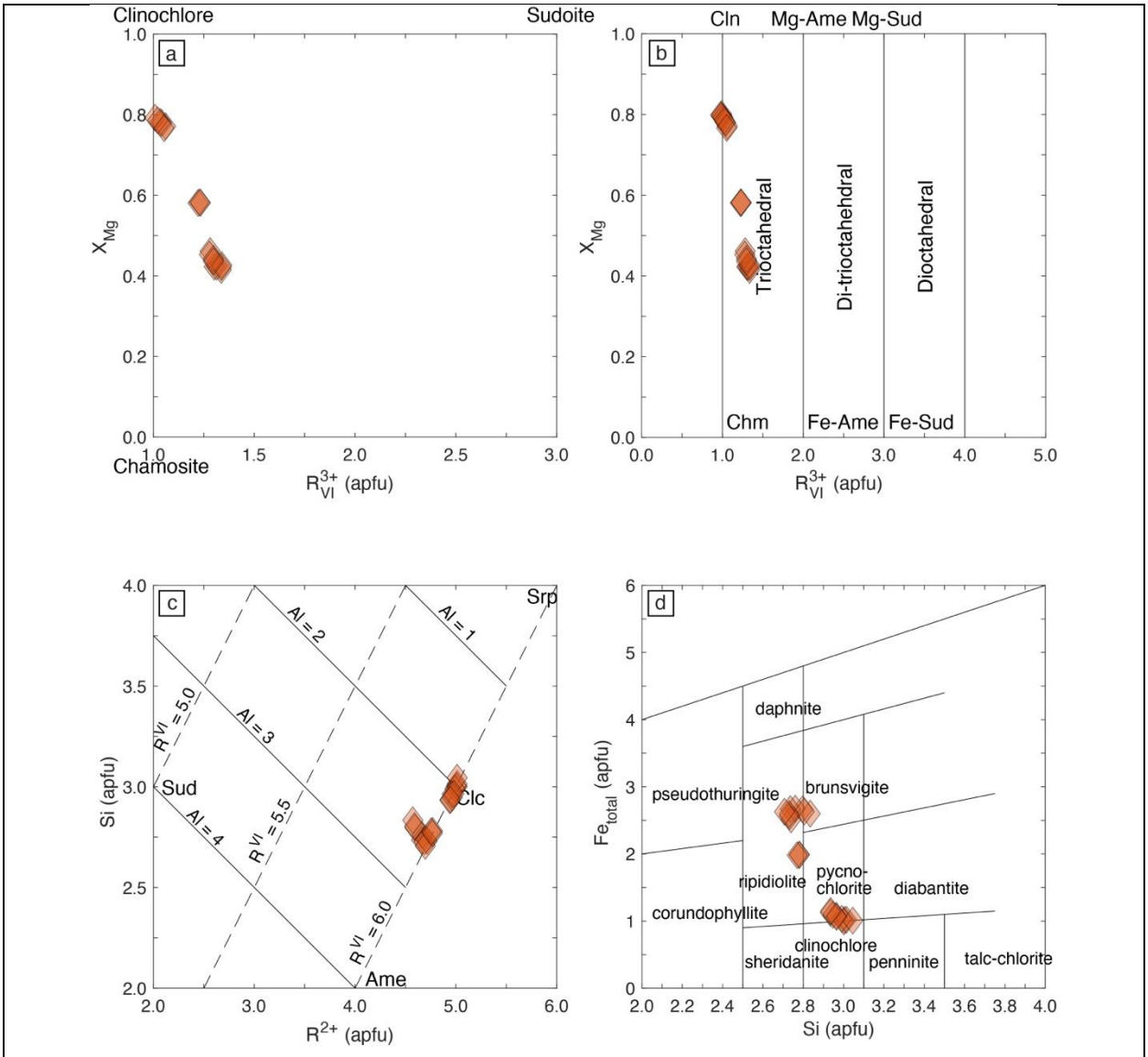

Figure 3.4.1 Chlorite compositional diagrams including plots of X_{Mg} vs $^{VI}R^{3+}$ (A, B), a plot of Si (apfu) vs R^{2+} (apfu) (C), and a plot of Fe_{total} (apfu) vs Si (apfu) (D). Data are from a chlorite schist black wall sample (SY404) and metasomatic garnet-omphacite-chlorite fels (SY462) from Syros, Greece (Walters *et al.*, 2019; 2021). Note that amesite is included in the plots for completion but amesite is not a member of the chlorite group. Figure 3.4.1(D) should not be used for classification.

Section 3.5: Chloritoid

Chloritoid is made up of two octahedral layers, L1 and L2, linked by SiO_4 tetrahedra, where L1 is (Na, Ca, Mg, Mn^{2+}, Fe^{2+})$_2$(Al,Ti,Fe^{3+})$O_2(OH)_4$, L2 is Al_3O_2, and the tetrahedral (*T*) site is 2[SiO_4] (See Table 3.5.1). Normalization depends on the treatment of Fe^{3+} and Fe^{2+} (see below). If H_2O is given as an input then the measured value is used, otherwise the ideal value of $(OH)_4$ is assumed.

Table 3.5.1 Example structural formula assignments for chloritoid

End-member	T	L2	L1	X_{Mg}
chloritoid (ctd)	Si,Si	Al,Al,Al	Al,Fe^{2+},Fe^{2+}	0
magnesiochloritoid (Mg-ctd)	Si,Si	Al,Al,Al	Al,Mg,Mg	1
ottrélite (otr)	Si,Si	Al,Al,Al	Al,Mn^{2+},Mn^{2+}	0

3.5.1 Fe-Mn valence options – Ferric iron can either be prescribed or estimated by charge balance criteria. If a prescribed value is used, then Fe^{3+} and Fe^{2+} can either be included in the input data (either as FeO and Fe_2O_3 or by including a column labeled *Fe3_ratio*) or assigned a global $Fe^{3+}/\Sigma Fe$ ratio. If the Fe^{3+} option is not selected, then the chloritoid formula will be calculated as $\Sigma Fe = Fe^{2+}$. In these cases, normalization is conducted based on 14 oxygen equivalents if H_2O is included as an input or 12 oxygen equivalents if H_2O is not known.

Ferric iron can also be estimated by charge balance. At low Fe^{3+}, the OH site is close to filled, but may be less than the ideal sum in Fe^{3+}-rich chloritoid, consistent with deprotonation and oxidation of Fe^{2+} to Fe^{3+} (Deer, Howie, and Zussman, 2013). While the assumption of 8 cations and 12 oxygen equivalents (anhydrous) used here to calculate Fe^{3+} is violated at elevated Fe^{3+} (which may occupy up to 50% of R^{3+} in the L1 layers), such high Fe^{3+} chloritoid compositions are rare (Deer, Howie, and Zussman, 2013). The calculation procedure used here is expected to perform well for most chloritoid analyses.

For manganese, $\Sigma Mn = Mn^{2+}$.

3.5.2 Plotting – Chloritoid compositions may be plotted as either a X_{Mg} binary or in the Fe^{2+}-Mg-Mn ternary (Fig. 3.5.1).

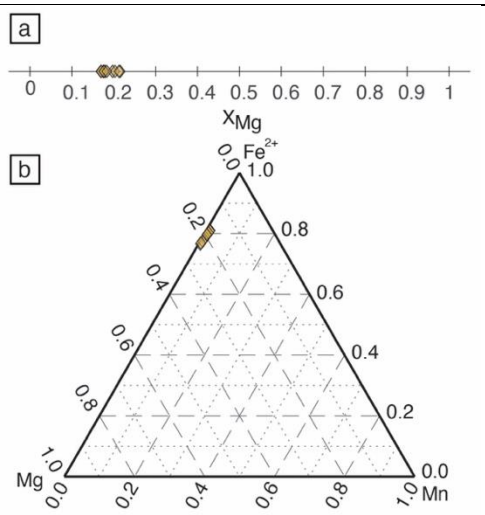

Figure 3.5.1 Binary X_{Mg} (A) and ternary Fe^{2+}, Mg, and Mn (B) compositional diagrams for chloritoid. Analytical data were collected on chloritoid inclusions in garnet cores in eclogite from As Sifah, Oman. Figure from Walters (2022).

Section 3.6: Cordierite

Cordierite ($A_{0\text{-}1}B_2T2_3T1_6O_{18}$) is calculated here normalized to 18 moles of oxygens. Cations are assigned as A = Ca, Na, and K, B = Fe^{2+}, Mn^{2+}, and Mg, T2 = Al and Ti, and T1 = Si, Al, and Fe^{3+}. The fraction of magnesium (X_{Mg}) is calculated as $Mg/(Mg+Fe^{2+})$. Cordierite can also incorporate Li, Be, H_2O, and CO_2; however, these elements are not routinely measured and are not considered here. Exchange vectors in Figure 3.6.1c can be used to identify Be and Li in the absence of measurement of these elements (Bertoldi *et al*., 2004). Example site assignments are given in Table 3.6.1.

Table 3.6.1 Example structural formula assignments for cordierite

End-member	T1	T2	B	A
cordierite	Si,Si,Si,Si,Si,Al	Al,Al,Al	Mg,Mg	
sekaninaite	Si,Si,Si,Si,Si,Al	Al,Al,Al	Fe^{2+},Fe^{2+}	
Manganicordierite	Si,Si,Si,Si,Si,Al	Al,Al,Al	Mn^{2+},Mn^{2+}	

3.6.1 Fe-Mn valence options – Fe^{3+} and Fe^{2+} can be included in the input data (either as FeO and Fe_2O_3 or by including a column labeled *Fe3_ratio*) or assigned a global $Fe^{3+}/\Sigma Fe$ ratio. If the Fe^{3+} option is not selected, then the chlorite formula will be calculated with $\Sigma Fe = Fe^{2+}$.

The blue color of cordierite originates from a charge-transfer between octahedrally coordinated Fe^{2+} and tetrahedrally coordinated Fe^{3+}, as a result most cordierite contains some fraction of Fe^{3+} (Geiger *et al*., 2000). A combined Mössbauer and electron paramagnetic resonance (EPR) study by Geiger *et al*. (2000) showed that Fe^{3+} primarily substitutes on the T1 site. As a result, Fe^{3+} is only allowed to substitute on T1 here. Natural Mg-cordierite were found to have less than 0.004 apfu Fe^{3+} (Geiger *et al*., 2000). Therefore, $\Sigma Fe = Fe^{2+}$ is a reasonable approximation for many natural cordierite samples.

One proposed mechanism for the incorporation of Fe^{3+} is through charge balance by substitution of Na within the center of the six-membered rings of the cordierite structure (Deer, Howie, and Zussman, 2013). However, Na incorporation can also couple to other potential substitution mechanisms and high Na contents in cordierite do not uniquely indicate elevated Fe^{3+} (Fig. 3.6.1).

For manganese, $\Sigma Mn = Mn^{2+}$.

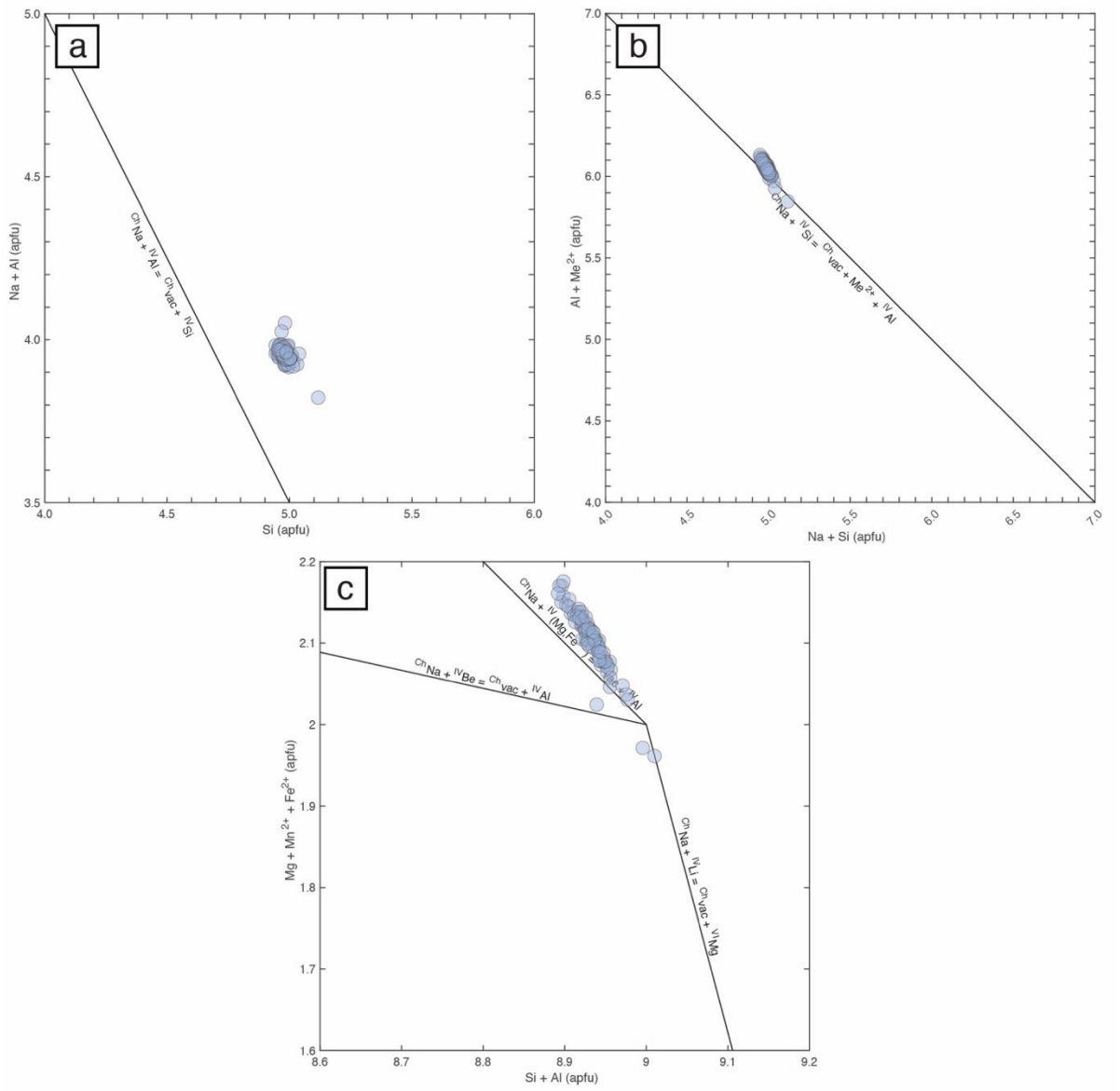

Figure 3.6.1 Plots of (a) Na + Al (apfu) vs Si (apfu), (b) of Al + Me^{2+} (divalent cations, apfu) vs Na + Si (apfu), and (c) Mg + Mn^{2+} + Fe^{2+} (apfu) vs Si + Al (apfu) for cordierite. Data are from Sorcar *et al.* (2020).

3.6.2 Plotting – Three plots are available for cordierite. First, the diagram of Na + Al (apfu) vs Si (apfu) after Tropper et al. (2018) explores the substitution mechanism $^{A}Na^{+} + {}^{IV}Al^{3+} = {}^{A}\square + {}^{IV}Si^{4+}$ (Fig. 3.6.1a). Second, the plot of Al + Me^{2+} (divalent cations, apfu) vs Na + Si (apfu) after Wolfsdorff and Schreyer (1992) explores the substitution mechanism $^{A}Na^{+} + {}^{B}\square + {}^{IV}Si^{4+} = {}^{A}\square + {}^{B}Me^{2+} + {}^{IV}Al^{3+}$ (Fig. 3.6.1b). Finally, the diagram of Mg + Mn^{2+} + Fe^{2+} (apfu) vs Si + Al (apfu) after (Bertoldi et al., 2004) can be used to identify potential Li and Be substitution if these elements are not measured (Fig. 3.6.1c).

Section 3.7: Epidote

Compositions of epidote group members are described as $A_2M_3T_3(O,OH,F)_{13}$, where A = K, Na, Ca, Sr, Mg, Mn^{2+}, and Fe^{2+}, M = Mg, Mn^{2+},Fe^{2+},Mn^{3+},Fe^{3+}, Cr, Ti, and ^{VI}Al, and T = ^{IV}Al and Si. If H_2O is measured and included as an input then the measured value will be used, otherwise OH = 1 is assumed. Normalization is based on a 12.5 oxygen equivalent (anhydrous) basis if H_2O is not included, otherwise normalization is based on 13 oxygen equivalents. Magnesium, Mn^{2+}, and $Fe^{2+}$are equipartitioned such that X_{Mg} ($Mg/(Mg + Mn^{2+} + Fe^{2+})$), X_{Mn} ($Mn^{2+}/(Mg + Mn^{2+} + Fe^{2+})$), and X_{Fe} ($Fe^{2+}/(Mg + Mn^{2+} + Fe^{2+})$) ratios are equal for M and A cations. An example site assignment is given in Table 3.7.1.

The most abundant epidote group minerals fall between the (clino-)zoisite ($Ca_2Al_3Si_3O_{11}O(OH)$) and epidote ($Ca_2Al_2Fe^{3+}Si_3O_{11}O(OH)$) endmembers. The exchange vectors with piemontite ($Ca_2Al_2Mn^{3+}Si_3O_{11}O(OH)$) and Cr-epidote ($Ca_2Al_2CrSi_3O_{11}O(OH)$) are also considered here. Endmembers fractions are expressed as (clino-)zoisite ($X_{czo} = (Al^{VI}-2)/(Fe^{3+} + Al^{VI} + Cr + Mn^{3+} - 2)$), epidote ($X_{ep} = Fe^{3+}/(Fe^{3+} + Al^{VI} + Cr + Mn^{3+} - 2)$), piemontite ($X_{pmt} = Mn^{3+}/(Fe^{3+} + Al^{VI} + Cr + Mn^{3+} - 2)$), and Cr-epidote ($X_{Crep.} = Cr/(Fe^{3+} + Al^{VI} + Cr + Mn^{3+} - 2)$).

Table 3.7.1 Example structural formula assignments for epidote

Endmember	T	M	A
(Clino-)Zoisite (czo/zo)	Si,Si,Si	Al,Al,Al	Ca,Ca
Epidote (ep)	Si,Si,Si	Al,Al,Fe^{3+}	Ca,Ca
Piemontite (pmt)	Si,Si,Si	Al,Al,Mn^{3+}	Ca,Ca
“Cr-Epidote (Cr-ep)”	Si,Si,Si	Al,Al,Cr	Ca,Ca

3.7.1 Fe-Mn valence options – Ferric Fe and Mn^{3+} can be calculated from ratios (input file or global) or from weight percent FeO, Fe_2O_3, MnO, and Mn_2O_3 values in the input file (see Section 2).

3.7.2 Plotting – Epidote compositions can be plotted in two ways. First, Xep can be plotted in an Al-Fe^{3+} binary diagram (similar to Fig. 3.5.1a for chloritoid X_{Mg}). Alternatively, epidote can be plotted on the allanite diagram (e.g., Fig. 3.1.1). However, analyses are plotted along the X axis only because Y+REE+U+Th = 0 for output from the epidote function and therefore Y = 0. The result is that the allanite diagram and the binary Al-Fe^{3+} diagram is effectively the same.

Section 3.8: Feldspar

Feldspar (AT_4O_8) is calculated here by normalizing to 8 oxygen equivalents, with A = Ca, Na, K, Sr, Ba, Fe^{2+}, Mn, and Mg and T = Al and Si at the tetrahedral site. Endmembers are calculated for anorthite (X_{an} = Ca/(Ca + Na + K)), albite (X_{ab} = Ca/(Ca + Na + K)), and alkali feldspar (X_{or} = K/(Ca + Na + K)). An example site assignment is given in Table 3.8.1.

Table 3.8.1 Example structural formula assignments for feldspar

Endmember	T	A
anorthite (an)	Si,Si,Al,Al	Ca
albite (ab)	Si,Si,Si,Al	Na
orthoclase (or)	Si,Si,Si,Al	K

3.8.1 Fe-Mn valence options – The feldspar calculation scheme uses $\Sigma Fe = Fe^{2+}$ and $\Sigma Mn = Mn^{2+}$. As a result, the calculation scheme is not appropriate for ferrisanadine-like compositions.

3.8.2 Plotting – Plotting is available as the classic An-Ab-Or feldspar ternary, with and without subdivisions (Fig. 3.8.1). If feldspar subdivisions are selected, the fields for the discredited feldspar intermediate species are plotted: bytownite (bytw, X_{an} = 70-90), labradorite (labr, X_{an} = 70-90), andesine (ands, X_{an} = 30-50), oligoclase (olig, X_{an} = 10-30), and anorthoclase (ano, X_{or}= 10-36). Note that the abbreviations for the intermediate subdivisions used here are not included in Warr (2021) as they are discredited. Boundaries for the feldspar subdivision are commonly drawn either, 1. Maintaining a fixed X_{an} and X_{or}, or 2. Maintaining constant proportion of X_{an}:X_{ab} at varying X_{or} and constant proportion of X_{or}:X_{ab} at varying X_{an}. Here the latter is chosen, and the subdivision boundaries are not parallel to X_{an} and X_{or} (Fig. 3.8.1b). These boundaries should not be used for classification and are provided for historical reasons.

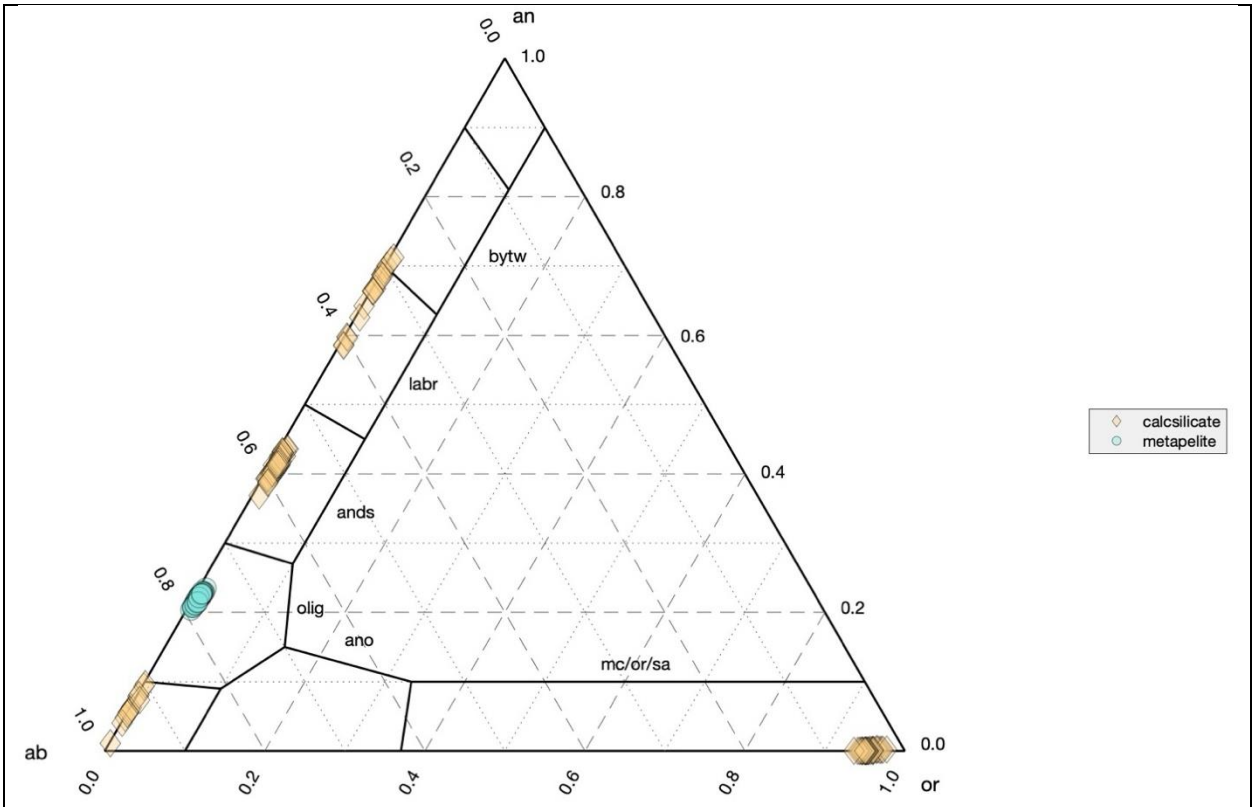

Figure 3.8.1 Feldspar ternary plot with data color coded by rock type using the advanced plot module. Data from Walters et al. (2022) are grouped by lithology. Plagioclase in metapelite samples show a restricted compositional range, whereas plagioclase from calcsilicates span X_{an} = 0 to 0.7.

Section 3.9: Garnet

Garnet ($X_3Y_2Z_3O_{12}$) has a flexible structure and can incorporate a variety of elements in its four atomic sites (Grew *et al*., 2013). Here the compositional space is restricted to those elements which are abundant in most natural garnets and can be measured on the EPMA: X = Na, Ca, Mg, Mn, Fe^{2+}, and Y at the dodecahedral site, Y = Fe^{2+}, Mg, Mn, Fe^{3+}, Cr, Ti, Al, and excess Si at the octahedral site, Z = Fe^{3+}, Al, and Si at the tetrahedral site, and O_2 at the anion site. The hydrogarnet substitution, $4H + {}^{z}\square \rightarrow \square + {}^{z}Si$, may be significant in garnets along the grossular-katoite join but is not considered here. Garnet structural formula are calculated using normalization to 8 cations and 12 oxygens for Fe^{3+}-estimation, or 12 oxygen basis alone for all other calculation schemes for Fe^{3+} (see below). Cation assignment follows the order given by Grew *et al*. (2013) and does not consider equipartitioning of Fe^{2+}, Mg, and Mn between the dodecahedral and octahedral sites.

There are two garnet calculation routines: 1. A simplified scheme for most garnet compositions, and 2. A more complex recalculation and endmember calculation scheme for Ti-rich garnets with significant schorlomite and/or morimotoite components. Checking *Ti_Endmembers* under *MineralSpecificOptions* will enable the Ti-garnet specific calculation. In both cases, Fe^{3+} can be given in the input, set as a global value, or estimated by charge balance. Both recalculation schemes are mathematically equivalent until cations are assigned to the structural formula and endmembers are calculated, thus the cation apfu values are equal. Example site assignments are given in Table 3.9.1.

3.9.1 Simplified recalculation – In the simplified recalculation scheme, Fe^{3+} is unlikely to be assigned to the tetrahedral site. First, Si and ${}^{IV}Al$ are assigned to the tetrahedral site. Aluminum is added until the sum of the tetrahedral site is 3. Ferric iron is only assigned to the tetrahedral site in the rare event that Si + Al < 3, which may only occur in very Al-poor garnets. Otherwise, Fe^{3+} is only assigned to the octahedral site.

Endmember fractions are calculated using the matrix inversion method for solving systems of linear equations:

(**3.9.1**) $X_{Endmembers} = M^{-1} \cdot A_T$

Where $X_{Endmembers}$ is the matrix of endmember fractions, M^{-1} is a matrix of the ideal moles of the cations for each endmember, and A_T is the transposed matrix of Ca, Mg, ΣFe, Cr, Mn, and Al cations for each analysis. Following Equation 3.9.1, the sum of the endmembers is calculated and normalized to unity. Equation 3.9.1 is convenient for rapidly solving large systems of linear equations; however, only square matrices are invertible, and the technique is not appropriate for all endmember calculations. The garnet endmembers considered are almandine (X_{alm}), spessartine (X_{sps}), grossular (X_{grs}), pyrope (X_{prp}), andradite (X_{adr}), and uvarovite (X_{uv}).

Table 3.9.1 Example structural formula assignments for garnet

End-member	Z	Y	X
almandine (alm)	Si,Si,Si	Al,Al	Fe^{2+},Fe^{2+},Fe^{2+}
spessartine (sps)	Si,Si,Si	Al,Al	Mn^{2+},Mn^{2+},Mn^{2+}
grossular (grs)	Si,Si,Si	Al,Al	Ca,Ca,Ca
pyrope (prp)	Si,Si,Si	Al,Al	Mg,Mg,Mg

andradite (and)	Si,Si,Si	Fe^{3+}, Fe^{3+}	Ca,Ca,Ca
uvarovite (uv)	Si,Si,Si	Cr,Cr	Ca,Ca,Ca
morimotoite (mmt)	Si,Si,Si	Ti,(Fe^{2+},Mg)	Ca,Ca,Ca
schorlomite(slo)	Si,Fe^{3+},Fe^{3+}	Ti,Ti	Ca,Ca,Ca

3.9.2 Ti-garnet recalculation – In the Ti-garnet recalculation scheme, Fe^{3+} can be added to the tetrahedral site through the schorlomite substitution. First, the difference between the ideal 3 cations on the tetrahedral site and Si are calculated. Second, 3-Si on the tetrahedral site is subtracted from the sum of Ti + Al + Fe^{3+} + Cr, which gives the total tri- and tetravalent cations on the octahedral site. The remaining cations on the octahedral site are divalent. The total divalent cations on the octahedral site are calculated as 2 minus the sum of Ti + Al + Fe^{3+} + Cr adjusted in the previous step. It is assumed that Ti substitution is either through a morimotoite or schorlomite substitution. The morimotoite substitution considered here is $2\,^{VI}Al^{3+} = Ti^{4+} + {}^{VI}Me^{2+}$ where $^{VI}Me^{2+}$ can be Fe^{2+}, Mn^{2+}, or Mg. Therefore, the Ti on the octahedral site associated with the morimotoite substitution is equal to the total sum of divalent cations on the octahedral site calculated in the previous step. The schorlomite substitution is $Si^{4+} + {}^{VI}Al^{3+} = {}^{IV}Fe^{3+} + Ti^{4+}$. As a result, $^{IV}Fe^{3+}$ is equal to the total Ti apfu minus the total sum of divalent cations on the octahedral site. This calculation assumes that Fe^{3+} is the only Me^{3+} cations assigned to the tetrahedral by coupled substitution with Ti.

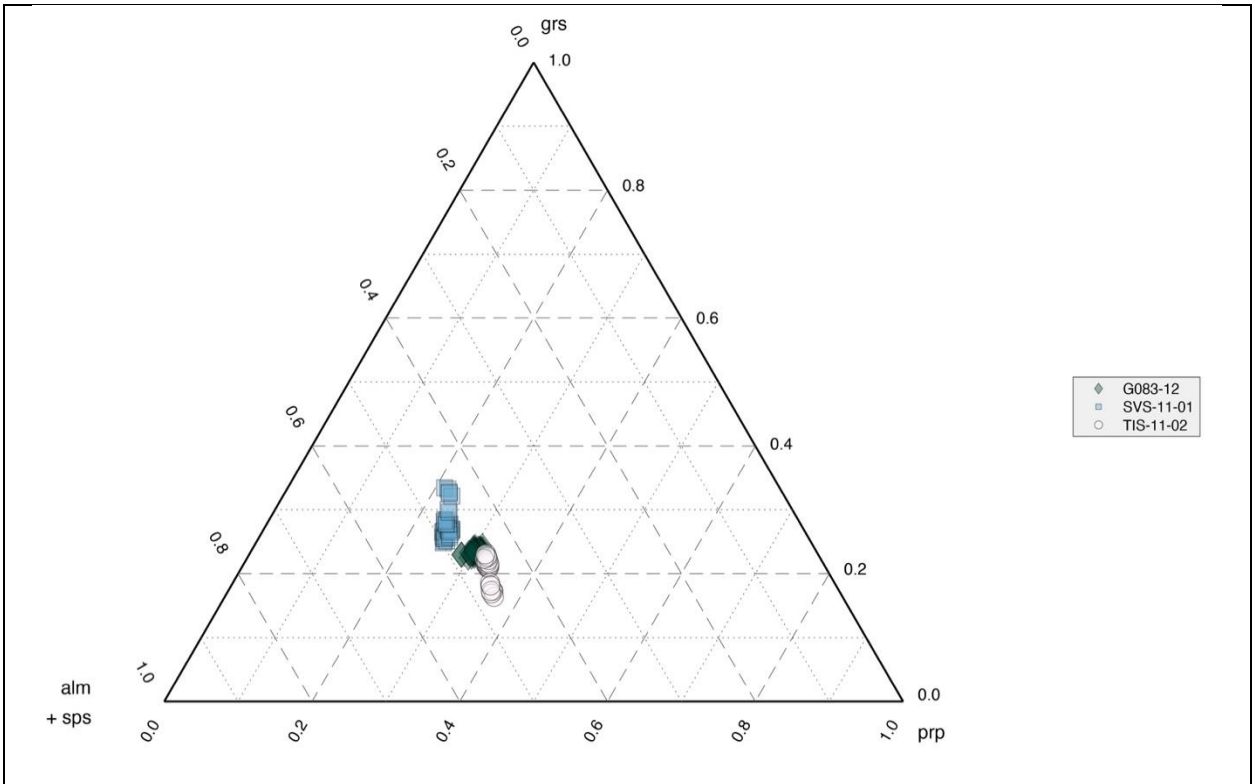

Figure 3.9.1 Ternary grossular, almandine + spessartine, and pyrope diagram with garnet compositional data from three metagabbroic eclogite samples (data from Walters et al., 2019; 2021).

The fraction of the schorlomite endmember (X_{slo}) is calculated from the fraction of $^{IV}Fe^{3+}$ on the tetrahedral site, whereas the remaining endmembers are calculated from/normalized to the fraction of Si on the tetrahedral site. Endmembers with tetrahedral Si are further subdivided by the occupation of the octahedral site with morimotoite calculated as $X_{mmt} = (Ti + {}^{VI}Me^{2+})/(2 - {}^{IV}Fe^{3+} - {}^{IV}Al)$, andradite as $X_{adr} = {}^{VI}Fe^{3+}/(2 - {}^{IV}Fe^{3+} - {}^{IV}Al)$, uvarovite as $X_{uv} = Cr/(2 - {}^{IV}Fe^{3+} - {}^{IV}Al)$, and Al-garnet as $^{VI}Al/(2 - {}^{IV}Fe^{3+} - {}^{IV}Al)$, where Al-garnet corresponds to all endmembers with Al on the octahedral site. The fraction of Al garnet is then multiplied by the fractions of Fe^{2+}, Mg, Mn^{2+}, and Ca on the dodecahedral site for X_{alm}, X_{prp}, X_{sps}, and X_{grs}.

3.9.3 Fe-Mn valence options – Ferric iron can either be prescribed or estimated by charge balance criteria. If a prescribed value is used, then Fe^{3+} and Fe^{2+} can either be included in the input data (either as FeO and Fe_2O_3 or by including a column labeled *Fe3_ratio*) or assigned a global $Fe^{3+}/\Sigma Fe$ ratio. If the Fe^{3+} option is not selected, then the garnet formula will be calculated with $\Sigma Fe = Fe^{2+}$.

For manganese, $\Sigma Mn = Mn^{2+}$.

3.9.3 Plotting – Garnet compositions can be plotted in three ternaries. First, the $X_{alm} + X_{sps}$, X_{prp}, X_{grs} ternary (Fig. 3.9.1) represents the four most abundant endmember fractions in common metamorphic and igneous garnet. Almandine and spessartine are combined as garnets are typically enriched in both components at low temperature and enriched in the pyrope component at high temperatures. It is important to note that X_{sps} and X_{alm} do not perfectly co-vary, especially at low pressure and temperature conditions near the garnet-in reaction (*e.g.*, Caddick and Kohn, 2013), and restricting the 4-dimensional endmember composition space of common garnets to 3-dimensions will obscure compositional trends. Also available are ternary diagrams of $^{VI}Fe^{3+}$, Cr + Ti, and ^{VI}Al for substitutions at the octahedral site and the andradite-morimotite-schorlomite discrimination diagram after Grew *et al.* (2013) with compositional boundaries following the dominant-valency rule after Bosi *et al.* (2019) (Fig. 3.9.2).

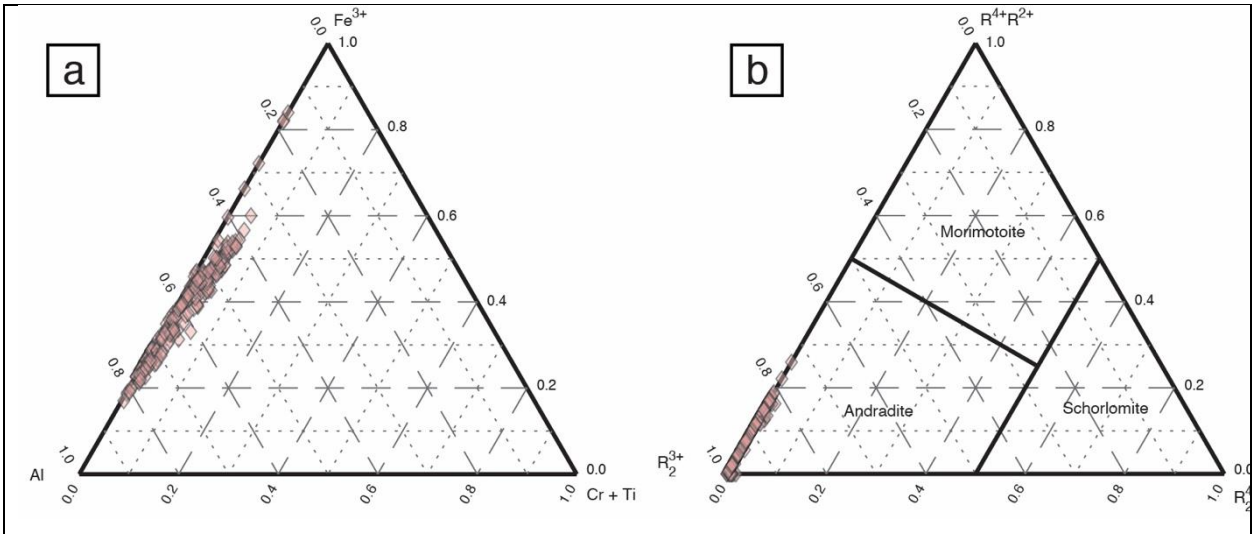

Figure 3.9.2 Ternary diagram of (a) $^{VI}Fe^{3+}$, Cr + Ti, and ^{VI}Al and (b) andradite-morimotite-schorlomite. Example data were collected on grossular-andradite skarn garnet from Xanthi, Greece (Walters, 2022).

Section 3.10: Ilmenite-hematite-bixbyite

Ilmenite group minerals and oxides with similar chemical formula (A_2O_3, *e.g.*, hematite, bixbyite) are calculated to 2 cations and 3 oxygen equivalents for Fe^{3+} estimation or 3 oxygen equivalents for all other options (see below). Here A = Fe^{2+}, Fe^{3+}, Mg, Mn^{2+}, Mn^{3+}, Cr, V, Ti, Si, and Ca. Silicon and Ca are primarily included as a monitor for mixed analysis with silicate phases. Since all cations are assigned to A there is no formal structural formula assignment, and the structural formula output is equal to the apfu output.

Endmembers are calculated for hematite (Fe_2O_3), ilmenite ($FeTiO_3$), pyrophanite (MnTiO3), and geikielite ($MgTiO_3$). The hematite component is calculated by $X_{hem} = Fe^{3+}/(Fe^{3+} + Ti)$ and the total ilmenite + pyrophanite + geikielite component is calculated by $1 - X_{hem}$. The remaining endmembers are calculated from the $Fe^{2+}/(Fe^{2+} + Mn^{2+} + Mg)$ for ilmenite (X_{ilm}), $Mn^{2+}/(Fe^{2+} + Mn^{2+} + Mg)$ for pyrophanite (X_{pph}), and $Mg/(Fe^{2+} + Mn^{2+} + Mg)$ for geikielite (X_{gk}).

3.10.1 Fe-Mn valence options – Ferric iron can either be prescribed or estimated by charge balance criteria. If a prescribed value is used, then Fe^{3+} and Fe^{2+} can either be included in the input data (either as FeO and Fe_2O_3 or by including a column labeled *Fe3_ratio*) or assigned a global $Fe^{3+}/\Sigma Fe$ ratio. If the Fe^{3+} option is not selected, then the ilmenite formula will be calculated with $\Sigma Fe = Fe^{2+}$.

For manganese, any combination of MnO and/or Mn_2O_3 and a ratio (*Mn3_ratio*) can be selected. If Fe^{3+} and Fe^{2+} are calculated by charge balance, then $\Sigma Mn = Mn^{2+}$. In most cases *Mn3_ratio* = 0 is appropriate.

3.10.2 Plotting – Currently no plotting option is available.

Section 3.11: Lawsonite

The structural formula of the lawsonite group is given as $AM_2T_2O_7(OH)_2 \cdot H_2O$ where A = K, Na, Ca, Sr, Mg, Mn^{2+}, and Fe^{2+}, M = Mg, Mn^{2+},Fe^{2+},Mn^{3+},Fe^{3+}, Cr, Ti, and ^{VI}Al, and T = ^{IV}Al and Si. If H_2O is measured and included as an input then the measured value will be used, otherwise values of OH = 2 and H_2O = 1 are assumed. If H_2O is included as an input, then the hydrous normalization of 10 oxygen equivalents is taken, otherwise the anhydrous normalization of 8 oxygen equivalents is used.

Magnesium, Fe^{2+}, and Mn^{2+} are not equipartitioned between A and M cations, instead Mg, Fe^{2+}, and then Mn^{2+} are sequentially assigned to the M cations until the site is full, with the remainder of these cations assigned to A. Example site assignments are shown in Table 3.11.1.

Table 3.11.1 Example structural formula assignments for lawsonite group minerals

Endmember	T	M	A
lawsonite	Si,Si	Al,Al	Ca
itoigawaite	Si,Si	Al,Al	Sr
hennomartinite	Si,Si	Al,Mn^{3+}	Ca

3.11.1 Fe-Mn valence options – Ferric Fe and Mn^{3+} can be calculated from a combination of ratios (input file or global) and weight percent FeO, Fe_2O_3, MnO, and Mn_2O_3 values in the input file (see Section 2).

3.11.2 Plotting – Lawsonite commonly shows some substitution of Fe, Ti, and Cr for Al. Two diagrams are given which differently show these substitutions (Fig. 3.11.1). First, an X-Y diagram of Fe^{3+} + Ti + Cr (apfu) vs. ^{VI}Al (apfu) is available. Second, 4xTi, Fe^{3+}, and Cr can be plotted in the ternary space.

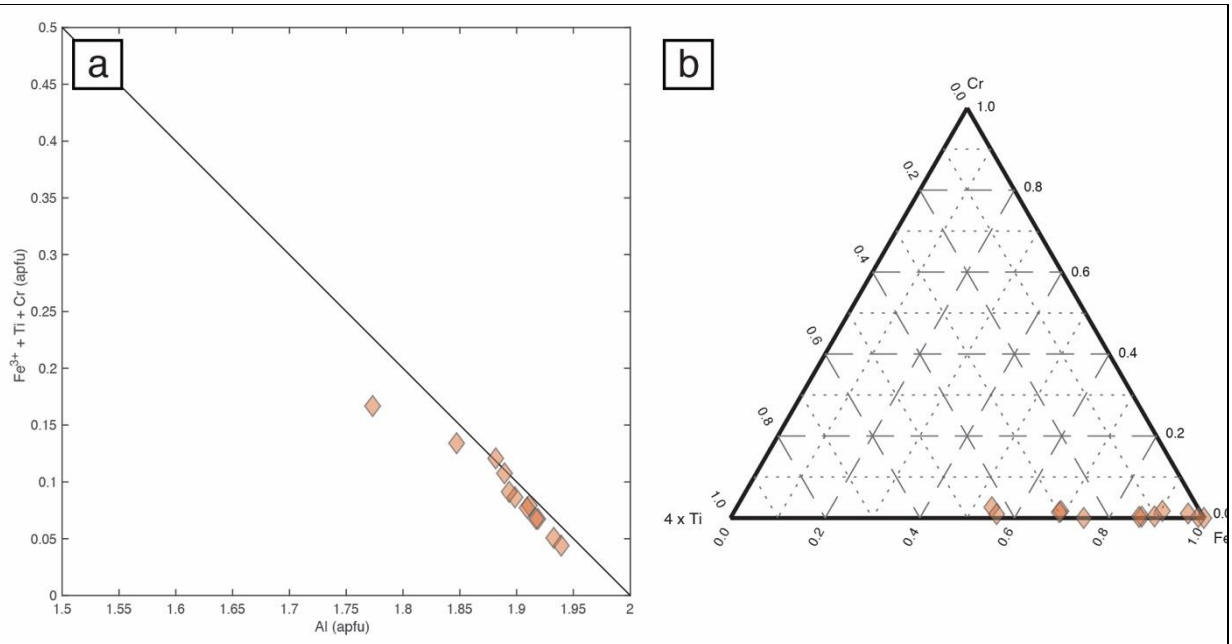

Figure 3.11.1 (a) X-Y diagram of Fe^{3+} + Ti + Cr (apfu) vs. ^{VI}Al (apfu) and (b) ternary diagram of 4xTi, Fe^{3+}, and Cr showing the distribution of M cations in lawsonite (unpublished data).

Section 3.12: Mica

Mica ($IM_{2-3}T_4O_{10}W_2$) is calculated here using the hydrous normalization to 12 oxygen equivalents (10O + 2OH). Ions are assigned as I = □, K, Na, Ca, and Ba, M = Mg, Mn, Fe^{2+}, $^{VI}Fe^{3+}$, Cr, Ti, and ^{VI}Al, T = ^{IV}Al, $^{IV}Fe^{3+}$, and Si, and W = F, Cl, and OH. While an important I cation in some mica species, Li is not considered here as it is not commonly measured. If H_2O is not measured, then the OH content is calculated as 2 - (F + Cl) and the calculated H_2O content is iterated 50 times to allow for convergence on the appropriate OH value, otherwise the known H_2O content from the input data used and the iteration is skipped. Example site assignments and species used for endmember calculations are given in Table 3.12.1.

Table 3.12.1 Example structural formula assignments for mica minerals

Endmember	W	T	M	I
muscovite (ms)	OH,OH	Si,Si,Si,Al	Al,Al	K
celadonite (cel)	OH,OH	Si,Si,Si,Si	Fe^{3+},Mg	K
ferroceladonite (cel)	OH,OH	Si,Si,Si,Si	Fe^{3+},Fe^{2+}	K
ferroaluminoceladonite (Alcel)	OH,OH	Si,Si,Si,Si	Al,Fe^{2+}	K
aluminoceladonnite (Alcel)	OH,OH	Si,Si,Si,Si	Al,Mg	K
paragonite (pg)	OH,OH	Si,Si,Si,Al	Al,Al	Na
margarite (mrg)	OH,OH	Si,Si,Al,Al	Al,Al	Ca
pyrophyllite (prl)	OH,OH	Si,.Si,Si,Si	Al,Al	
phlogopite (phl)	OH,OH	Si,Si,Si,Al	Mg,Mg,Mg	K
annite (ann)	OH,OH	Si,Si,Si,Al	Fe^{2+},Fe^{2+},Fe^{2+}	K
eastonite (eas)	OH,OH	Si,Si,Al,Al	Al,Mg,Mg	K
siderophyllite (sid)	OH,OH	Si,Si,Al,Al	Al,Fe^{2+},Fe^{2+}	K

3.12.1 Endmember calculation – Mica endmembers are calculated based on two compositional groups: 1. Dioctahedral muscovite (X_{ms}), celadonite (X_{cel}), aluminoceladonite (X_{Alcel}), paragonite (X_{pg}), margarite (X_{mrg}), and pyrophyllite (X_{prl}) species, or 2. Trioctahedral, phlogopite (X_{phl}), annite (X_{ann}), eastonite (X_{eas}), and siderophyllite (X_{sid}) species. The total dioctahedral or trioctahedral components are given as X_{DiOct} and X_{TriOct}, respectively.

The calculation procedure is as follows. First, if the sum of the M cations is greater than 2, then some trioctahedral component is possible and is calculated as $X_{TriOct} = \Sigma M - 2$ and $X_{DiOct} = 1 - X_{TriOct}$. The procedure is then divided based between dioctahedral and trioctahedral endmember calculations.

For dioctahedral micas, the muscovite, paragonite, margarite, and pyrophyllite have a total of two ^{VI}Al on M, whereas aluminoceladonite has one ^{VI}Al and celadonite has one $^{VI}Fe^{3+}$, as a result the total fraction of muscovite, paragonite, margarite, and pyrophyllite is calculated by $\Sigma_{ms,pg,mrg,prl} = (^{VI}Al + ^{VI}Fe^{3+}) - 1$ and the total celadonite content (Σ_{cel}) is the remaining fraction $\Sigma_{cel} = 1 - \Sigma_{ms,pg,mrg,prl}$. The celadonite fraction is calculated as $X_{cel} = (^{VI}Fe^{3+}/(^{VI}Al + ^{VI}Fe^{3+})) \cdot \Sigma_{cel}$ and the aluminoceladonite fraction is calculated as $X_{Alcel} = \Sigma_{cel} - X_{cel}$. Since pyrophyllite contains no I cations, total fraction of muscovite, paragonite, and margarite is represented by $\Sigma_{ms,pg,mrg} =$

(K + Na + Ca) · $\Sigma_{ms,pg,mrg,prl}$ and $X_{prl} = \Sigma_{ms,pg,mrg,prl} - \Sigma_{ms,pg,mrg}$. Finally, X_{ms}, X_{pg}, and X_{mrg} are calculated from $\Sigma_{ms,pg,mrg}$ using the fractions of K, Na, and Ca on I. Finally, the fractions are normalized such that the proportions of the dioctahedral endmembers are equal to X_{DiOct}.

For trioctahedral micas, the total fraction for the phlogopite-annite is first calculated as $\Sigma_{phl\text{-}ann} = Si - 2$ such that individual fractions of phlogopite and annite can be calculated: $X_{phl} = \Sigma_{phl\text{-}ann} \cdot X_{Mg}$ and $X_{ann} = \Sigma_{phl\text{-}ann} - X_{phl}$. The total fraction for the siderophyllite-eastonite is also calculated, $\Sigma_{sid\text{-}east} = 1 - \Sigma_{phl\text{-}ann}$, and the individual fractions for eastonite and siderophyllite are calculated: $X_{east} = \Sigma_{sid\text{-}east} \cdot X_{Mg}$ and $X_{sid} = \Sigma_{sid\text{-}east} – X_{east}$. Here X_{Mg} is calculated as $Mg/(Mg + Fe^{2+})$. Finally, the fractions are normalized such that the proportions of the trioctahedral endmembers are equal to X_{TriOct}.

3.12.2 Fe-Mn valence options – For Fe^{3+} and Fe^{2+} the user can either include FeO and Fe_2O_3 as input data or ΣFeO or ΣFe_2O_3 and a ratio. The $Fe^{3+}/\Sigma Fe$ ratio can be given in the input data for each analysis as *Fe3_ratio* or a by assigning a global ratio in the GUI to all analyses. If the Fe^{3+} option is not selected, then the mica formula will be calculated as $\Sigma Fe = Fe^{2+}$. Additionally, it is possible to give the fraction of Fe^{3+} on the tetrahedral site ($^{IV}Fe^{3+}/\Sigma Fe^{3+}$). The fraction of tetrahedral Fe^{3+} can be read as *tetra_Fe3* from the input file or a global value can be prescribed for all analyses (see Section 2). If no global value is given and *tetra_Fe3* is not in the input file, then the default $^{IV}Fe^{3+}/\Sigma Fe^{3+} = 0$ is assumed.

For micas stochiometric calculation of $Fe^{3+}/\Sigma Fe$ is not allowed for the following reasons: 1. Vacancies are possible at both the octahedral and 12-fold coordinated interlayer sites and 2. The estimation of Fe^{3+} by charge balance requires stoichiometric limits to be exceeded by excess cations calculated when assuming $\Sigma Fe = Fe^{2+}$, which is rarely the case for micas (Schumacher, 1991). Li *et al.* (2020) proposed a new method of Fe^{3+} estimation of biotite, using a machine learning-based principal component regression; however, Forshaw and Pattison (2021) found a poor fit between observed and predicted Fe^{3+} and Fe^{2+} contents, and the approach is therefore not implemented in MinPlotX.

For manganese, $\Sigma Mn = Mn^{2+}$.

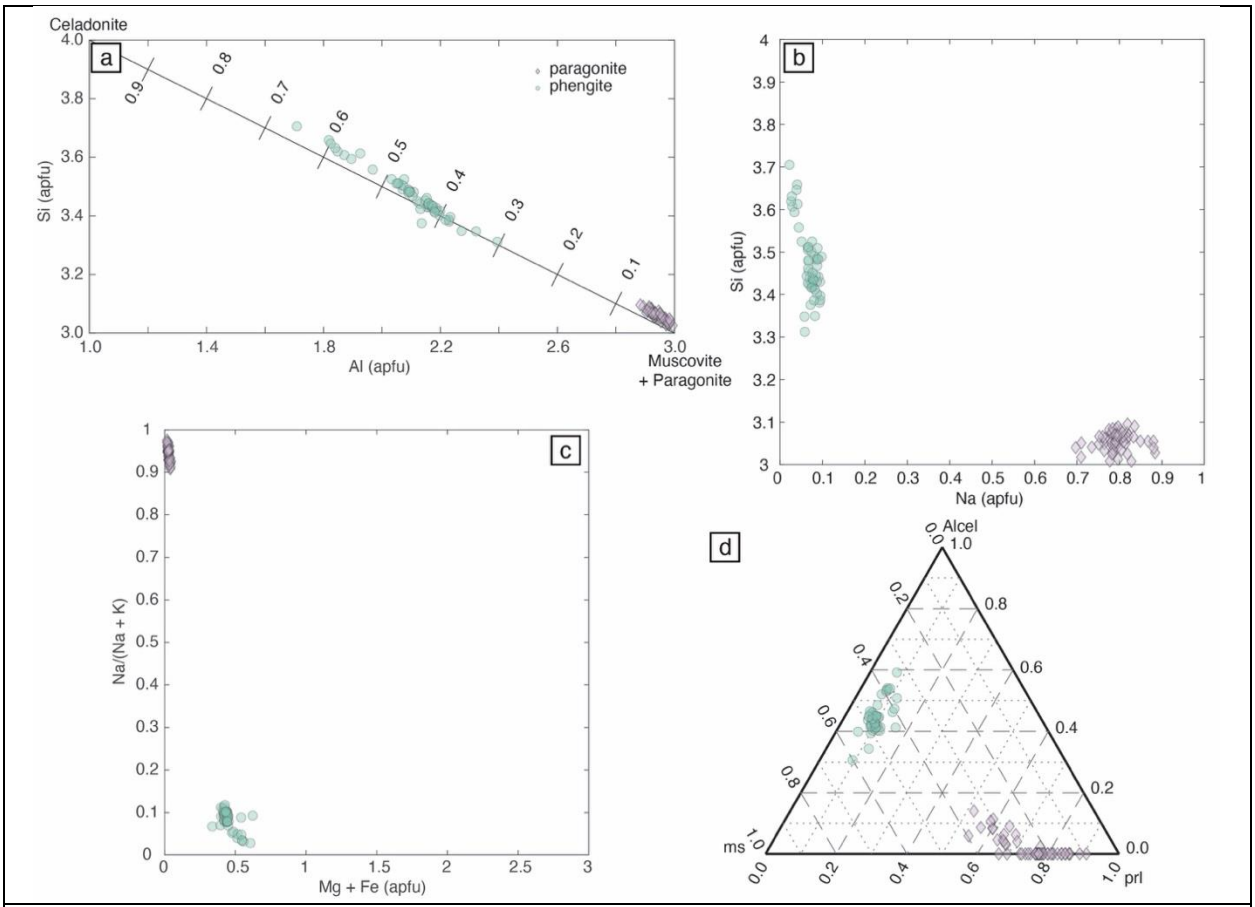

Figure 3.12.1 Plots include of (a) Si (apfu) vs Al (apfu), (b) Si (apfu) vs Na (apfu) (c), Na/(Na + K) vs Mg + Fe (apfu), and (d) the X_{prl}, X_{Alcel}, and X_{ms} ternary. Data from Xu *et al.* (2022) show the decreasing Si and Mg + Fe and increasing Al + Na between peak metamorphic and progressive retrograde generations of white mica.

3.12.3 Plotting – Six plots are available for mica. Plots include 1. Si (apfu) vs Al (apfu) showing solid solution between celadonite and muscovite + paragonite (Fig. 3.12.1a), 2. Si (apfu) vs Na (apfu) (Fig. 3.12.1b), 3. Na/(Na + K) vs Mg + Fe (apfu) (Fig. 3.12.1c), 4. trioctahedral Ann-Phl-Sid-East solid solution diagram of Al_M vs X_{Mg} (Fig. 3.12.2a), 5. the X_{prl}, X_{Alcel}, and X_{ms} ternary (Fig. 3.12.1d), and 6. F-Cl-OH ternary (Fig. 3.12.2b).

Analyses with > 50 % of the trioctahedral component are only plotted in the Na/(Na + K) vs Mg + Fe (apfu), Ann-Phl-Sid-East, and F-Cl-OH ternary diagrams. In contrast, analyses with < 50 % of the trioctahedral component are not plotted on the Phl-Sid-East diagram.

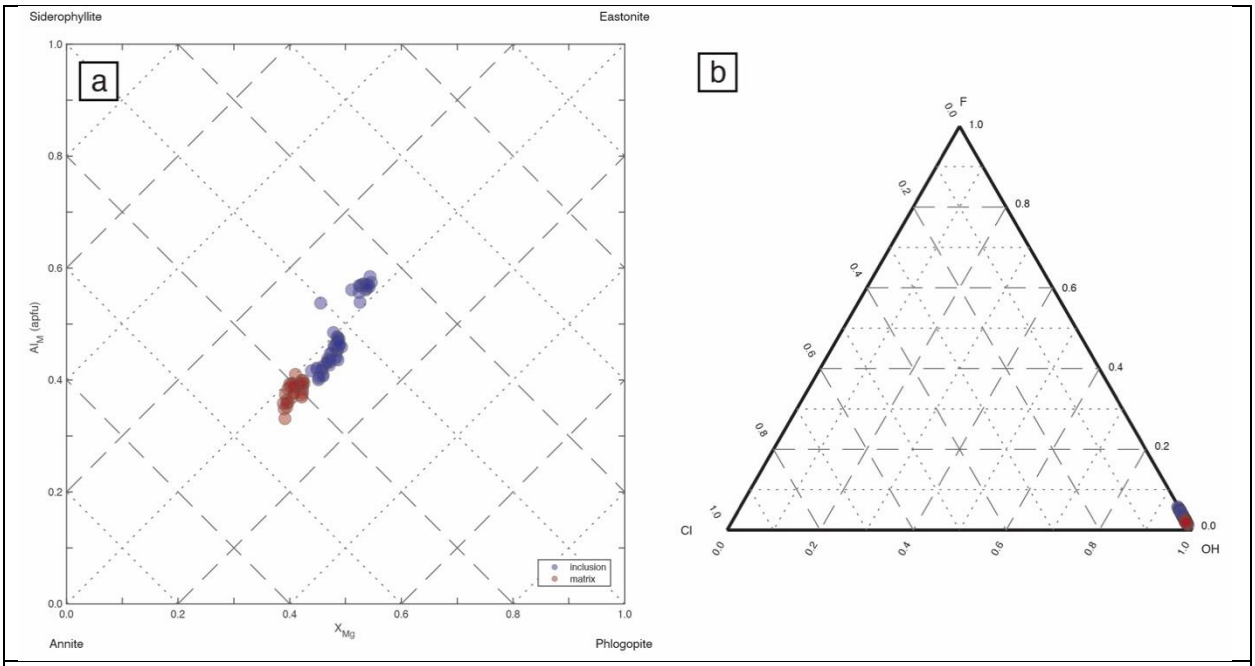

Figure 3.12.2 (a) trioctahedral Ann-Phl-Sid-East solid solution diagram of Al_M vs X_{Mg} and (b) F-Cl-OH ternary. Biotite data are grouped in the advanced plot module into biotite inclusions in garnet and matrix biotite. Inclusion biotite grains show preservation of higher of Al_M and X_{Mg} from the prograde to peak metamorphic history, whereas matrix biotite has reset to lower Al_M and X_{Mg} due to garnet breakdown by retrograde net transfer reactions (Walters *et al*., 2022). Inclusion biotite grains also contain elevated F relative to matrix grains.

Section 3.13: Olivine

Olivine (M_2TO_4) is calculated here with M = Ca, Mg, Mn^{2+}, Fe^{2+}, Ni, Cr, Fe^{3+}, Ti, and Al at the octahedral site, and T = Fe^{3+}, Al, and Si at the tetrahedral site. Normalization is to 3 cations and 4 oxygens in the Fe^{3+}-estimation routine, and on a 4-oxygen basis for all other calculation options (see below).

Endmember fractions are calculated using Equation 3.9.1 for forsterite (X_{fo}), fayalite (X_{fa}), tephroite (X_{te}), and calcio-olivine ($X_{Ca\text{-}ol}$). Example site assignments are given in Table 3.13.1 for endmember compositions.

Table 3.13.1 Example structural formula assignments for mica minerals

Endmember	T	M
forsterite (fo)	Si	Mg,Mg
fayalite (fa)	Si	Fe,Fe
tephroite (te)	Si	Mn,Mn
calcioolivine (Ca-ol)	Si	Ca,Ca

3.13.1 Fe-Mn valence options – Ferric iron can either be prescribed or estimated by charge balance criteria. If a prescribed value is used, then Fe^{3+} and Fe^{2+} can either be included in the input data (either as FeO and Fe_2O_3 or by including a column labeled *Fe3_ratio*) or assigned a global $Fe^{3+}/\Sigma Fe$ ratio. If the Fe^{3+} option is not selected, then the olivine formula will be calculated with $\Sigma Fe = Fe^{2+}$.

For manganese, $\Sigma Mn = Mn^{2+}$.

3.13.2 Plotting – Three plots are available for olivine (Fig. 3.13.1). First is an option for a binary plot of the forsterite content (Fig. 3.13.1a). Second, a ternary diagram in the X_{fo}, $X_{Ca\text{-}ol}$, and X_{fa} + X_{te} system is available (Fig. 3.13.1b). Finally, a plot with the Fo number on the x-axis and mass fraction of NiO (wt. %) on the y-axis is available (Fig. 3.13.1c).

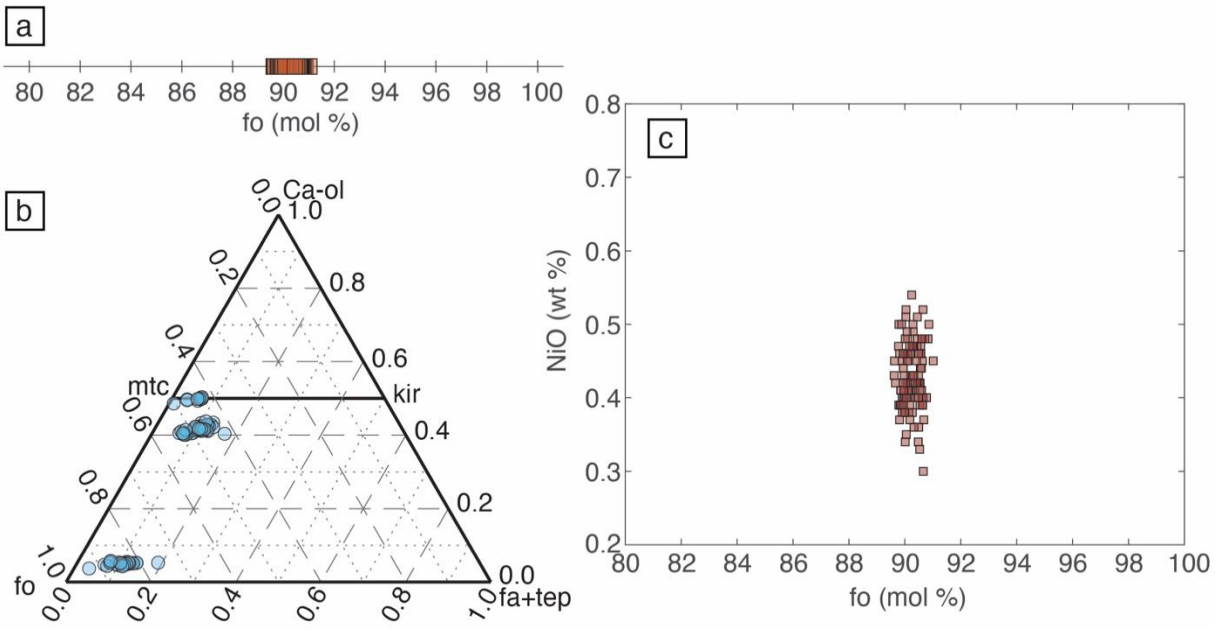

Figure 3.13.1 Binary forsterite (A), ternary forsterite, calcio-olivine, and fayalite + tephroite (B), and forsterite vs. NiO (wt %) (C) olivine compositional diagrams. Data in A and C are analyses of olivine from mantle peridotite, Wadi Fins, Oman (de Obseso and Kelemen, 2020). Data in B are analyses of experimentally grown olivine (Le Pioufle and Canil, 2012). Figure replicated from Walters (2022).

Section 3.14: Pyroxene

Pyroxene ($M2M1T_2O_6$) compositions are calculated following Morimoto *et al.* (1989), with K, Na, Ca, Fe^{2+}, Mg, and Mn^{2+} at the distorted octahedral *M*2 site, Fe^{2+}, Mg, Mn^{2+}, Cr, Fe^{3+}, Ti, and ^{VI}Al at the octahedral *M*1 site, and Fe^{3+}, ^{IV}Al, and Si at the tetrahedral site. Vanadium, Zn, and Sc may also substitute at the *M*1 site, but are typically observed at trace levels, whereas Li may substitute at *M*2 as a major element in spodumene but is not measurable by EPMA. These elements are not considered here. Ferrous iron, Mg, and Mn^{2+} are equipartitioned between *M*1 and *M*2 sites. Normalization is to 4 cations and 6 oxygens in the Fe^{3+}-estimation routine, and on a 6-oxygen basis for all other routines (see below). Example site assignments for endmember compositions are given in Tables 3.14.1 and 3.14.2.

Endmember fractions are calculated in three possible ways based on the check boxes in the *MineralSpecificOptions* area. First, if no box is checked then only wollastonite (X_{wo}), ferrosilite (X_{fs}), and enstatite (X_{en}) are calculated as Ca / (Ca + Mg + Fe^{2+}), Fe^{2+} / (Ca + Mg + Fe^{2+}), and Mg / (Ca + Mg + Fe^{2+}), respectively. Second, if the *Na_Endmembers* box is checked then the endmember calculation uses Equation 3.9.1 for wollastonite (X_{wo}), ferrosilite (X_{fs}), enstatite (X_{en}), jadeite (X_{jd}), aegirine (X_{aeg}), and kosmochlor (X_{kos}). In high pressure and/or temperature pyroxenes, the potassium clinopyroxene ($KAlSiO_2O_6$ and $KCrSi_2O_6$), calcium-Eskola ($Ca_{0.5}AlSi_2O_6$), and kushiroite (calcium-Tschermaks, $CaAlAlSiO_6$) components may significant (Harlow, 1999). If both the *Na_Endmembers* and *HighPT_Endmembers* boxes are checked the endmember calculation procedure of Harlow (1999) will be used. For this procedure, jadeite (X_{jd}), aegirine (X_{aeg}), diopside + hedenbergite (X_{dihd}), calcium-Tschermaks pyroxene (X_{ks}), kosmochlor (X_{kos}), K-kosmochlor (X_{Kkos}), K-jadeite (X_{Kjd}), calcium-Eskola pyroxene (X_{caes}), and enstatite (X_{en}) are calculated. In a change to the procedure of Harlow (1999), K is equipartitioned between X_{Kko} and X_{Kjd} endmembers. Abbreviations for endmembers are also after Harlow (1999).

Table 3.14.1 Example structural formula assignments for pyroxene

End-member	T	M1	M2
Wollastonite (wo)	Si,Si	Ca	Ca
Ferrosilite (fs)	Si,Si	Fe	Fe
Enstatite (en)	Si,Si	Mg	Mg
Jadeite (jd)	Si,Si	Al	Na
Aegirine (aeg)	Si,Si	Fe^{3+}	Na
Kosmochlor (kos)	Si,Si	Cr	Na

Table 3.14.2 Structural formula assignments for Harlow (1999) endmembers

End-member	T	M1	M2
Enstatite (en)	Si,Si	Mg	Mg
Diopside (di)	Si,Si	Mg	Ca
Hedenbergite (hd)	Si,Si	Fe	Ca
Jadeite (jd)	Si,Si	Al	Na
Aegirine (aeg)	Si,Si	Fe^{3+}	Na
Kushiroite (ks)	Si,Al	Al	Ca

kosmochlor (kos)	Si,Si	Cr	Na
"K-kosmochlor (K-kos)"	Si,Si	Cr	K
"K-jadeite (K-jd)"	Si,Si	Al	K
"Ca-Eskola (caes)"	Si,Si	Al	0.5Ca

3.14.1 Fe-Mn valence options – Ferric iron can either be prescribed or estimated by charge balance criteria. If a prescribed value is used, then Fe^{3+} and Fe^{2+} can either be included in the input data (either as FeO and Fe_2O_3 or by including a column labeled *Fe3_ratio*) or assigned a global $Fe^{3+}/\Sigma Fe$ ratio. If the Fe^{3+} option is not selected, then the pyroxene formula will be calculated with $\Sigma Fe = Fe^{2+}$.

For manganese, $\Sigma Mn = Mn^{2+}$.

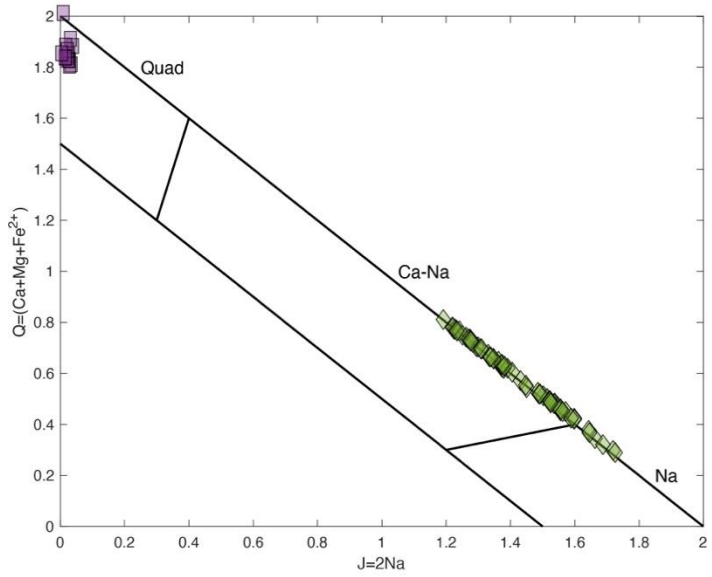

Figure 3.14.1 'Q-J' diagram after Morimoto *et al.* (1989) classifying Ca-Mg-Fe pyroxenes (Quad), Na-Ca pyroxenes (Na-Ca), and Na pyroxenes (Na). Example data in the 'Quad' field are clino- and orthopyroxene grains from gabbro-norite cumulate bodies and dikes from Alpine-Apennine ophiolites (purple squares, Piccardo and Guarnieri, 2011). Example data of Na- and Ca-Na clinopyroxene (green diamonds) are from a metasomatic garnet-omphacite-chlorite fels from Syros, Greece (SY462; Walters et al., 2019; 2021). Diagram reproduced after Walters (2022).

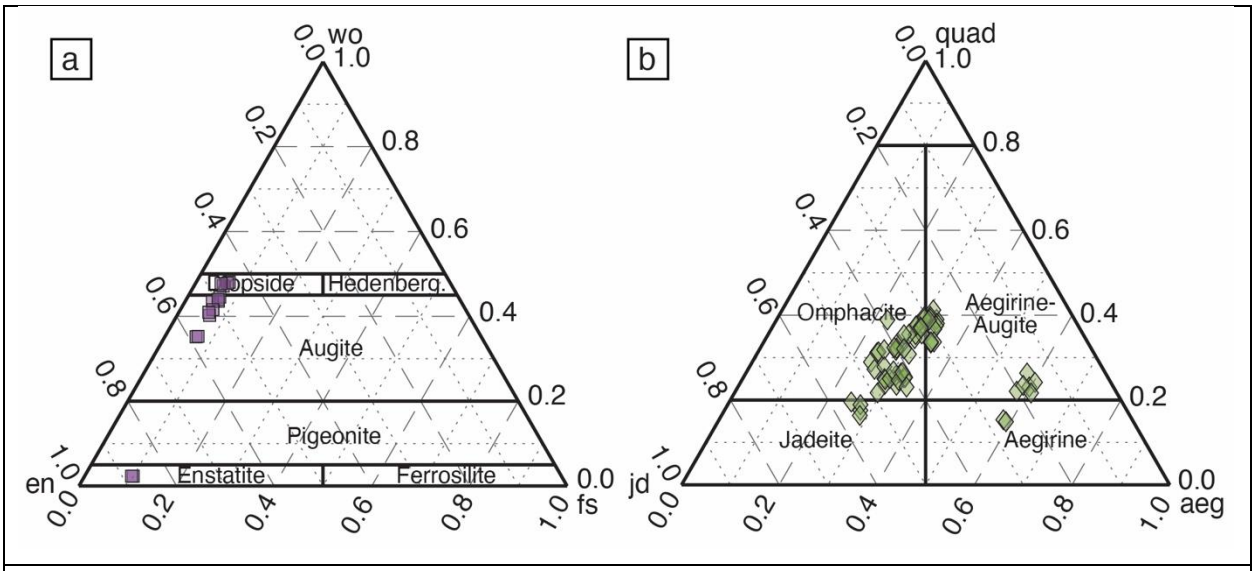

Figure 3.14.2 Ternary wollastonite, enstatite, and ferrosilite (A), and quad., jadeite, and aegirine (B) pyroxene compositional diagrams. Example data in A are clino- and orthopyroxene grains from gabbro-norite cumulate bodies and dikes from Alpine-Apennine ophiolites (Piccardo and Guarnieri, 2011). Example data in B are Na-clinopyroxene from a metasomatic garnet-omphacite-chlorite fels from Syros, Greece (SY462; Walters *et al*., 2019; 2021). Diagram reproduced after Walters (2022).

3.14.2 Plotting – Plotting and classification follows Morimoto *et al.* (1989). First, the so called 'Q-J' diagram distinguishes Ca-Mg-Fe pyroxenes (Quad), Na-Ca pyroxenes (Na-Ca), and Na pyroxenes (Na), where J = 2Na is plotted on the x-axis and Q = Ca + Mg + Fe^{2+} is plotted on the y-axis (see Fig. 3.14.1). For Ca-rich pyroxenes, the user may restrict endmember calculation and plotting to 'Quad' compositions, which is a useful approximation for many igneous pyroxenes. Discrimination plots also include the X_{wo}, X_{fs}, and X_{en}, (Fig. 3.14.2a) and X_{quad}, X_{jd}, and X_{aeg} (Fig. 3.14.2b) ternaries after Morimoto *et al.* (1989). Plots of X_{caes} and X_{ks} and $X_{K\text{-}cpx}$ ($X_{K\text{-}cpx} = X_{K\text{-}kos} + X_{K\text{-}jd}$) and X_{caes} following Harlow (1999) are also available (Fig. 3.14.3).

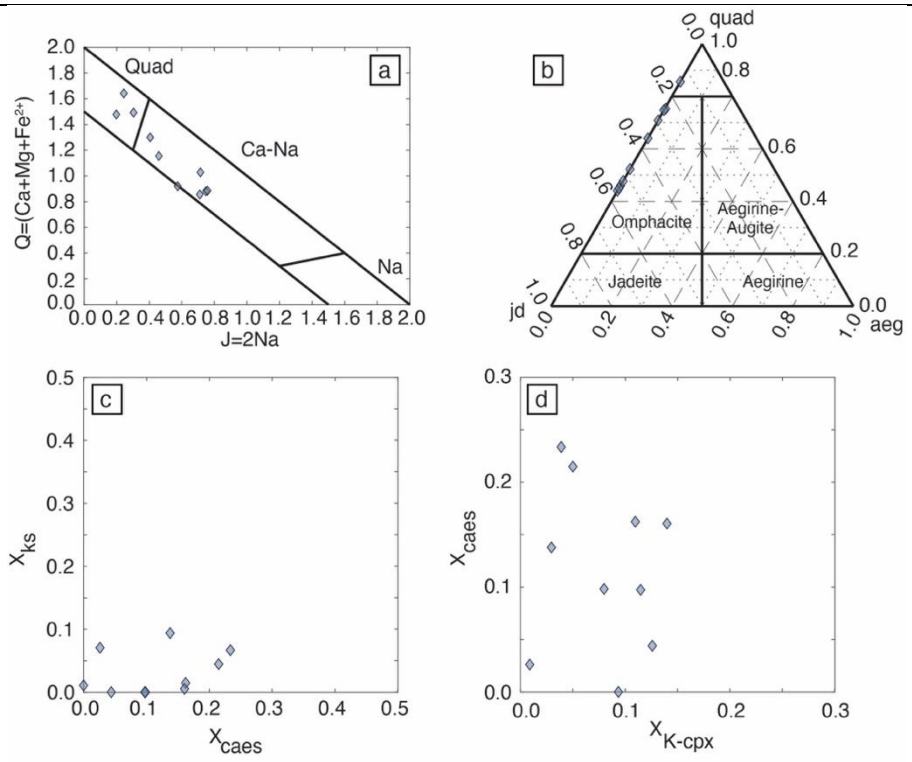

Figure 3.14.3 Pyroxene 'Q-J' (a) and quad-jadeite-aegirine ternary (b) as in previous figures. In addition, diagrams of X_{ks} vs X_{caes} (c) and X_{caes} vs X_{Kcpx} (d) after Harlow (1999) are shown here. Data are also from Harlow (1999) and the figure is reproduced after Walters (2022).

Section 3.15: Scapolite

Scapolite-group minerals have the general formula $M_4[T_{12}O_{24}]A$ where M = Ca, Sr, Ba, K, Na, Mg, Mn^{2+}, and Fe^{2+}, T = ^{IV}Al and Si, and A = Cl^{1-}, F^{1-}, CO_3^{2-}, and SO_4^{2-}. If CO_2 is measured then the 27 oxygen equivalents are used for normalization, otherwise the method of Ketcham (2015) for apatite is followed a 24 oxygen equivalents is used. After oxygen normalization the apfu are then normalized to 12 Si + Al. If CO_2 is not measured, then the carbon content is calculated as 1 - (Cl^{-1} + F^{-1} + SO_4^{-1}).

Scapolite solid solution involves the endmembers marialite ($Na_4[Al_3Si_9O_{24}]Cl$), meionite ($Ca_4[Al_6Si_6O_{24}]CO_3$), and silvialite (ideally $Ca_4[Al_6Si_6O_{24}]SO_4$). Endmember fractions are usually not reported, instead composition is reported as equivalents of anorthite (X_{Eqan} = (Al – 3)/3) and fraction of meionite (X_{me} = $\Sigma Me^{2+}/4$, where Me^{2+} are divalent metal cations), both of which are commonly calculated in the scapolite literature.

3.15.1 Fe-Mn valence options – The scapolite calculation scheme uses $\Sigma Fe = Fe^{2+}$ and $\Sigma Mn = Mn^{2+}$.

3.15.2 Plotting – Of the three known scapolite endmembers, two of them share the same ideal cation assignment; however, it is the anion site that easily displays the full compositional variation between endmembers. As a result, a ternary of CO_3^{2-}, SO_4^{2-}, and Cl^- is given as the default plot for scapolite.

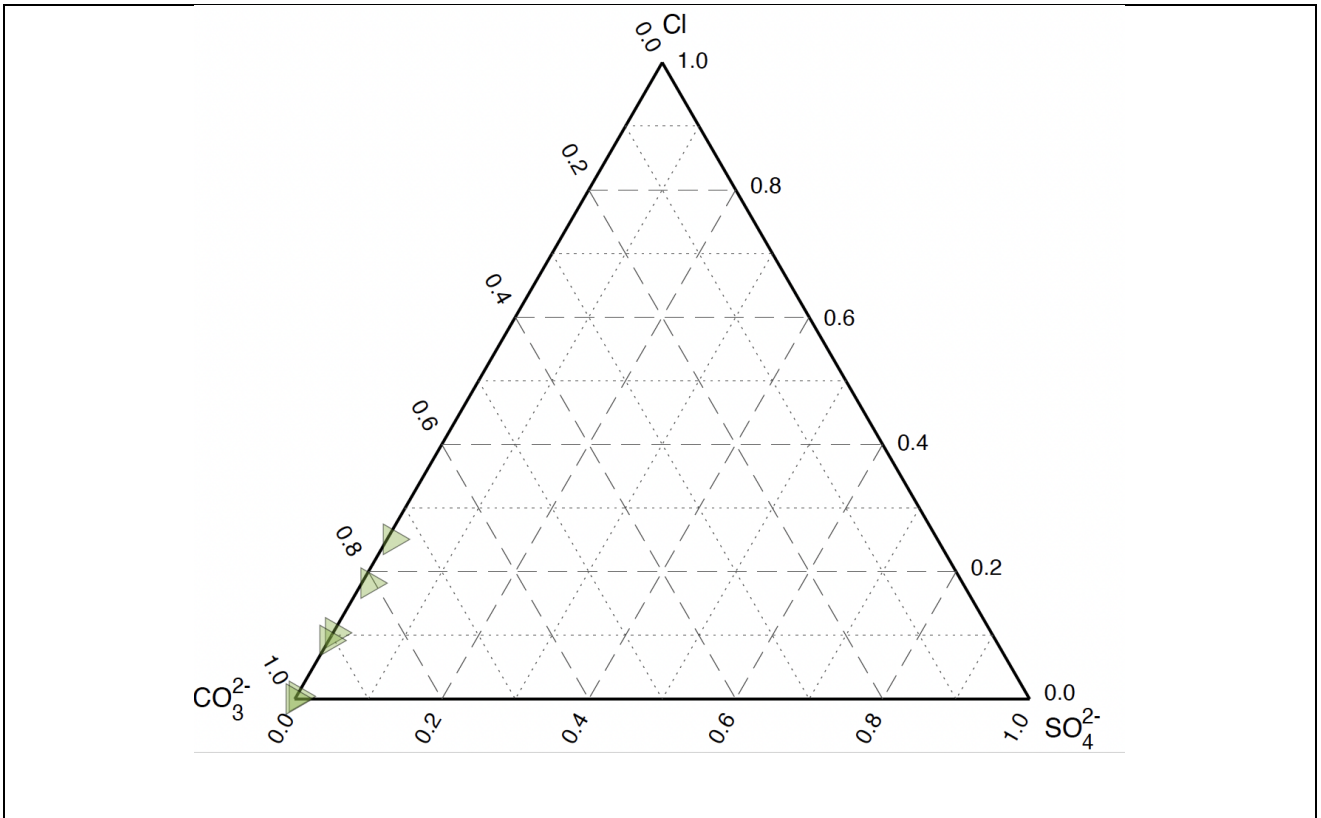

Figure 3.15.1 Ternary of CO_3^{2-}, SO_4^{2-}, and Cl^- of scapolite data from Walters & Kohn (2014).

Section 3.16: Serpentine

Serpentine ($M_6T_4O_{10}(OH)_8$) is structural formulae are calculated as assigned as M = Mg, Ca, Mn^{2+}, Fe^{2+}, $^{VI}Fe^{3+}$, Ni, Cr, Ti , and ^{VI}Al at the octahedral site, whereas T = ^{IV}Al, $^{IV}Fe^{3+}$, and Si at the tetrahedral site (Table 3.16.1). If H_2O is measured a hydrous normalization to 18 oxygen equivalents is used, otherwise an anhydrous normalization to 14 oxygen equivalents is used.

Table 3.16.1 Example structural formula assignments for serpentine

End-member	T	M
antigorite/chrysotile/lizardite	Si,Si,Si,Si	Mg,Mg,Mg,Mg,Mg,Mg
ferro-antigorite/chrysotile/lizardite	Si,Si,Si,Si	Fe^{2+},Fe^{2+},Fe^{2+},Fe^{2+},Fe^{2+},Fe^{2+}
caryopilite	Si,Si,Si,Si	Mn^{2+},Mn^{2+},Mn^{2+},Mn^{2+},Mn^{2+},Mn^{2+}
népouite/pecoraite	Si,Si,Si,Si	Ni,Ni,Ni,Ni,Ni,Ni

3.16.1 Fe-Mn valence options – Ferric iron and Fe^{2+} can be included in the input data (either as FeO and Fe_2O_3 or by including a column labeled *Fe3_ratio*) or assigned a global $Fe^{3+}/\Sigma Fe$ ratio. If the Fe^{3+} option is not selected, then the serpentine formula will be calculated as $\Sigma Fe = Fe^{2+}$. Additionally, it is possible to give the fraction of Fe^{3+} on the tetrahedral site ($^{IV}Fe^{3+}/\Sigma Fe^{3+}$). The fraction of tetrahedral Fe^{3+} can be read as *tetra_Fe3* from the input file or a global value can be prescribed for all analyses (see Section 2). If no global value is given and *tetra_Fe3* is not in the input file, then the default $^{IV}Fe^{3+}/\Sigma Fe^{3+} = 0$ is assumed.

For manganese, $\Sigma Mn = Mn^{2+}$.

3.16.2 Plotting – No default plotting options are currently available for serpentine.

Section 3.17: (Oxy)Spinel

Oxyspinel group minerals ($A^{2+}B_2^{3+}O_4$) are calculated here to 3 cations and 4 oxygen equivalents for Fe^{3+} estimation or 4 oxygen equivalents in all other cases (see below). Here A = Mg, Mn^{2+}, Fe^{2+}, Co, Zn, Ni, Ti, and Si at the tetrahedral site and B = Mg, Fe^{2+}, Fe^{3+}, Cr, V^{3+}, and Al at the octahedral site.

The structural formula calculation begins assignment of Al, V^{3+}, Cr, and Fe^{3+} to B. The remaining space on the B site is calculated as 2 - (Al + V^{3+}+ Cr + Fe^{3+}). The sum of Si + Ti > 0 is then the Fe^{2+} and Mg assigned to the B site is calculated as (Si + Ti) · X_{Fe} and (Si + Ti) · X_{Mg}, respectively, where X_{Fe} = $Fe^{2+}/(Fe^{2+}$ + Mg) and X_{Mg} = $Mg/(Fe^{2+}$ + Mg). The result is that Fe^{2+} and Mg are equipartitioned between A and B to maintain a constant proportion. Then rest of the elements, as well as the remaining Fe^{2+} and Mg, are assigned to A.

3.17.1 Endmember calculation – Endmembers fractions are determined by first calculating the fractions of Al, V, Cr, Fe^{3+}, and Fe^{2+} + Mg on the B site to calculate the total fractions of spinel-like, coulsonite-like, chromite-like, magnetite-like, and ulvöspinel-like groups of endmembers, respectively. The fractions of Fe^{2+}, Mg, Mn^{2+}, Ni, Zn, and Co are then multiplied to each group, resulting in equipartitioning of these elements between each of the groups calculated from the B-site stoichiometry. This procedure calculates a total of 28 different endmembers. The equipartitioning assumption is fictitious and will depend on the ordering of elements; however, the procedure used here is required accurately reproduce the correct endmember fractions for nearly pure oxyspinel phases.

3.17.2 Fe-Mn valence options – Ferric iron can either be prescribed or estimated by charge balance criteria. If a prescribed value is used, then Fe^{3+} and Fe^{2+} can either be included in the input data (either as FeO and Fe_2O_3 or by including a column labeled *Fe3_ratio*) or assigned a global $Fe^{3+}/\Sigma Fe$ ratio. If the Fe^{3+} option is not selected, then the pyroxene formula will be calculated with $\Sigma Fe = Fe^{2+}$.

For manganese, $\Sigma Mn = Mn^{2+}$.

3.17.3 Plotting – Oxyspinel compositions are plotted in the Cr, Fe^{3+} + 2Ti, and Al and Fe^{2+}, Mg, and Mn + Zn + Ni ternary diagrams (Fig. 3.17.1).

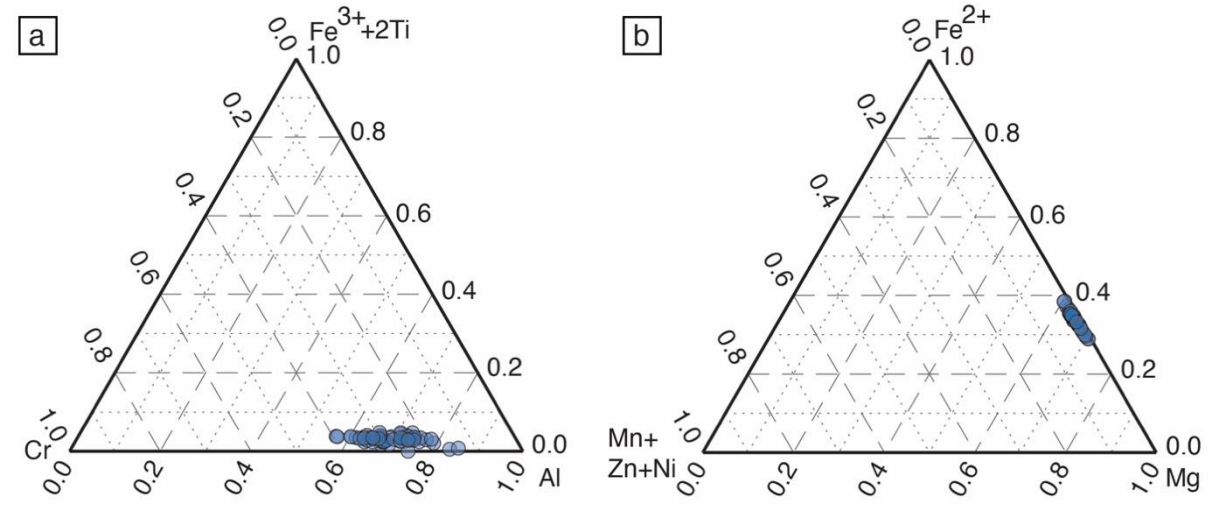

Figure 3.17.1 Ternary Fe^{3+} + 2Ti, Al, and Cr (A) and Fe^{2+}, Mg, and Mn + Zn + Ni (B) diagrams for spinel. Data are analyses of spinel from mantle peridotite, Wadi Fins, Oman (de Obseso and Kelemen, 2020). Figure is reproduced from Walters (2022).

Section 3.18: Staurolite

Staurolite ($A_4B_4C_{18}D_4T_8O_{40}X_8$) exhibits a complex formula with vacancies on multiple sites: A = Fe^{2+}, Mg, and □, B = Zn, Co, Mg, Li, Al, Fe^{3+},Mn, and □, C = Al, Fe^{3+}, Cr, V, Mg, and Ti, D = Al, Mg, and □, T = Si and Al, and X = OH, Cl, F, and O^{2-} (Hawthorne *et al*., 1993). Normalization can be done in two ways. First, the cations are normalized to 48 oxygen equivalents. If H_2O is not included as an input, then OH is calculated as 4 - (F + Cl) over 50 iterations. Staurolite is commonly normalized to Si + Al = 25.53 apfu following Holdaway et al. (1991). The option to normalize to Si + Al is available as the check box *Cation_Normalization* under the *MineralSpecificOptions* window. If H_2O content is given as an input is used, otherwise the OH content is calculated as 96 minus the sum of the charges of each cation. If the normalization factor is less than 1, this procedure can overfill the anion site (e.g., OH > 4); therefore, the anion sum is an important indicator of the quality of the analysis. Holdaway et al. (1991) estimates an uncertainty of 0.8 apfu (2σ) on the OH estimate using this approach. The total number of vacancies is then calculated as vac = 30 - cation total (Holdaway et al., 1991).

3.18.1 Fe-Mn valence options – Ferric iron and Fe^{2+} can be included in the input data (either as FeO and Fe_2O_3 or by including a column labeled *Fe3_ratio*) or assigned a global $Fe^{3+}/\Sigma Fe$ ratio. If the Fe^{3+} option is not selected, then the staurolite formula will be calculated as $\Sigma Fe = Fe^{2+}$. The values of 0.035 for ilmenite-bearing rocks ($X_{hem} < 0.10$) and 0.070 for hematite-ilmenite rocks ($X_{hem} > 0.10$) following Holdaway et al. (1991) are recommended.

For manganese, $\Sigma Mn = Mn^{2+}$.

3.18.2 Plotting – No plots are currently available for staurolite.

Section 3.19: Talc

The structural formula for talc ($M_3T_4O_{10}(OH)_2$) with M = K, Na, Ca, Mg, Mn, Fe^{2+}, Ni, Cr, Ti, and ^{VI}Al allocated to the octahedral site, and T = ^{IV}Al and Si at the tetrahedral site. If H_2O is included as an input a hydrous normalization to 12 oxygen equivalents is used, otherwise the anhydrous normalization to 11 oxygen equivalents is used.

3.19.1 Fe-Mn valence options – Ferric iron and Fe^{2+} can be included in the input data (either as FeO and Fe_2O_3 or by including a column labeled *Fe3_ratio*) or assigned a global $Fe^{3+}/\Sigma Fe$ ratio. If the Fe^{3+} option is not selected, then the talc formula will be calculated as $\Sigma Fe = Fe^{2+}$. Additionally, it is possible to give the fraction of Fe^{3+} on the tetrahedral site ($^{IV}Fe^{3+}/\Sigma Fe^{3+}$). The fraction of tetrahedral Fe^{3+} can be read as *tetra_Fe3* from the input file or a global value can be prescribed for all analyses (see Section 2). If no global value is given and *tetra_Fe3* is not in the input file, then the default $^{IV}Fe^{3+}/\Sigma Fe^{3+} = 0$ is assumed.

For manganese, $\Sigma Mn = Mn^{2+}$.

3.19.2 Plotting – No default plotting options are currently available for talc.

Section 3.20: Titanite

Titanite ($CaTiSiO_5$) has three structural sites and may display significant compositional variability. The 7-fold decahedral site may incorporate K, Na, Y, and Ca, the octahedral site may incorporate Mg, Mn, Fe^{3+}, Ti, and ^{VI}Al, and the tetrahedral site contains Si and ^{IV}Al. Rare Earth elements, Sr, Pb, and U may also substitute into the decahedral site, as well as Zr, Nb, and Ta on the octahedral site, but are not considered here due to their relatively low abundance in most titanite. Titanite are normalized to fully occupied octahedral and tetrahedral sites:

(**3.20.1**)

$$NF^C = \frac{2}{\sum_i^Z n_{Oct}^C + \sum_i^Z n_T^C}$$

Where NF^C is the cation-based normalization factor, $\sum_i^Z n_{Oct}^C$ is the sum of Mg, Mn, Fe^{3+}, Ti, and ^{VI}Al, and $\sum_i^Z n_T^C$ is the sum of Si and ^{IV}Al. Fluorine and OH^- are thought to substitute for O via the exchange vector $(Al,Fe)^{3+} + (OH,F)^- = Ti^{4+} + O^{2-}$ (see review in Kohn, 2017). Fluorine may be measured by directly EPMA; whereas, OH is calculated as $OH = (Al^{VI} + Fe^{3+}) - F$. Oxygen is calculated as the sum of the cation charges minus 0.5(F + OH). Finally, the fraction of titanite is calculated as $X_{ttn} = Ti/\sum_i^Z n_{Oct}^C$.

3.20.1 Fe-Mn valence options – The titanite formula recalculation scheme assumes $\Sigma Fe = Fe^{3+}$ and $\Sigma Mn = Mn^{2+}$.

3.20.2 Plotting – First, a plot of Ti (apfu) vs $^{VI}(Al + Fe^{3+})$ (apfu) shows the major substitutions on the octahedral site (Fig. 3.19.1a). A second plot of F (apfu) vs $^{VI}(Al + Fe^{3+})$ (apfu) can be used to illustrate whether F or OH is coupled to the substitution of Al and Fe^{3+} (Fig. 3.19.1b). Both diagrams are designed after Franz and Spear (1985).

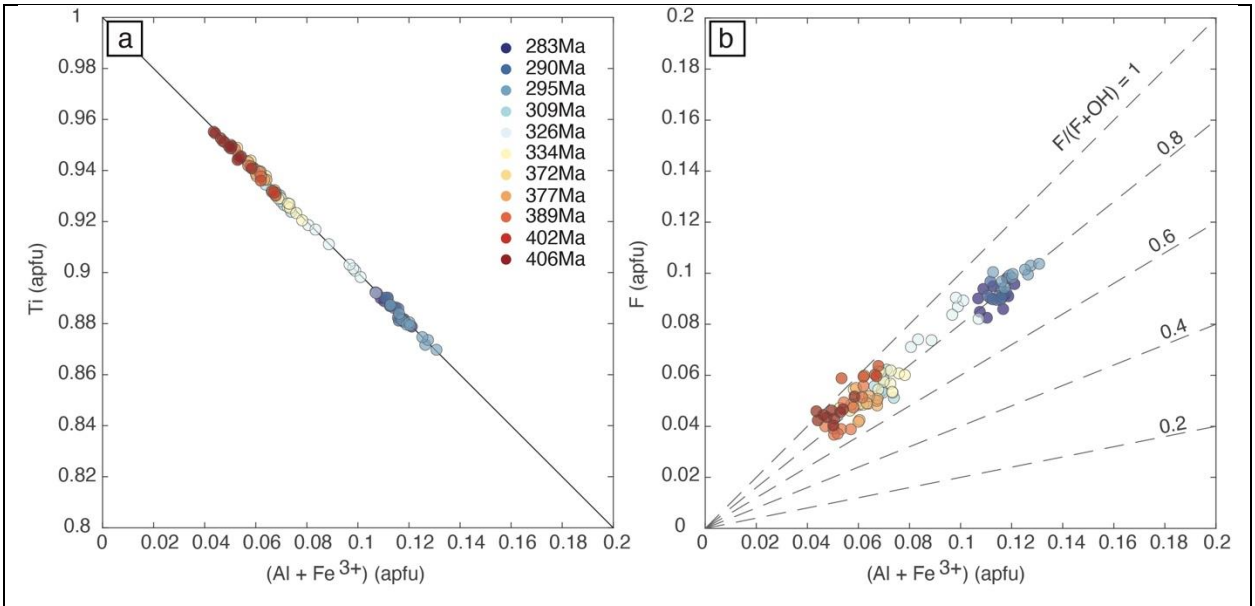

Figure 3.19.1 (a) Plot of Ti (apfu) vs $^{VI}(Al + Fe^{3+})$ (apfu), and (b) F (apfu) vs $^{VI}(Al + Fe^{3+})$ (apfu). Data from Walters *et al.* (2022) are plotted and color-coded by the associated single-spot U-Pb age measured by LA-ICP-MS for the same analytical region. These data show an increase

in F and $^{VI}(Al + Fe^{3+})$ between 400 and 290 Ma, with a slight decrease in F/(F + OH) from 1.0 to 0.8.

Section 3.21: Sulfides

A generic procedure is available for sulfide minerals. The datafile requires the mass fractions (in wt. %) for S, Co, Cu, As, Fe, Ni, Pb, and Zn. All elements, except for S, are optional, allowing the maximum flexibility for a variety of sulfides. Under the *MineralSpecificOption*s window the user can select *cation_normalization* for a cation-based recalculation, otherwise an anion-based normalization is chosen. In both cases the user can specify the number of *moles* to which the apfu will be normalized. Cation normalization works well for many sulfides but should not be done for pyrrhotite ($Fe_{1-x}S$) where the cation total is not fixed.

Under the *MineralSpecificOption*s window the user can also specify whether they want As (–3 to +5) to be treated as an anion or as a cation. On the reduced end As^{1-} may substitute for S_2^{2-} anion in pyrite and other disulfides. However, at more oxidizing conditions As^{2+} and As^{3+} may substitute for divalent and trivalent cations (*e.g*., Deditus *et al*., 2008; Qian *et al*., 2013). Trends in Fe-As-S ternary space may be used to determine whether As should be treated as a cation or anion for a given analysis (*e.g*., Deditus *et al*., 2014). The user can also use the sulfide recalculation and choose to treat As as an anion for the recalculation of arsenide minerals. Currently no compositional diagrams are available for specifically for sulfide phases; however, most common sulfide diagrams (e.g., atomic proportions of Cu, Fe, S ternary) can be easily plotted using the visualization module (*VisModule*) or the advanced plotting module (*AdvancedPlotModule*) under the *Results* tab.

Section 4: Generic formula recalculation procedure.

A generic formula recalculation procedure is available, as well as a sulfide specific version. To select the generic procedure the user must select *unknown* from the *mineral* dropdown menu. The user can specify whether they want a cation- or anion-based normalization procedure. The anion-based normalization is given as a default. If the user wants to select a cation-based calculation they must check the *cation_normalization* box under the *MineralSpecificOptions* window. Regardless of choice, the user can specify the number of *moles* to which the apfu will be normalized.

The user can specify Fe^{3+}, Fe^{2+}, Mn^{3+}, and/or Mn^{2+} by checking the *calculate with Fe3+* and/or *calculate with Mn3+* boxes. The user can either give the oxides of these elements for their respective valence states, a ratio in the input data (with data column headers of *Fe3_ratio* and *Mn3_ratio*), or by checking the box that allows for a global ratio assigned to all analyses.

References

Bailey, S.W. (1988). Chlorites: structures and crystal chemistry. *Reviews in Mineralogy and Geochemistry*, 19, 347-403.

Bertoldi, C., Proyer, A., Garbe-Schönberg, D., Behrens, H., & Dachs, E. (2004). Comprehensive chemical analyses of natural cordierites: implications for exchange mechanisms. *Lithos*, 78, 389-409.

Bosi, F., Hatert, F., Hålenius, U., Pasero, M., Miyawaki, R., & Mills, S.J. (2019). On the application of the IMA–CNMNC dominant-valency rule to complex mineral compositions. *Mineralogical Magazine*, 83, 627-632.

Deditius, A.P., Reich, M., Kesler, S.E., Utsunomiya, S., Chryssoulis, S.L., Walshe, J., & Ewing, R.C. (2014). The coupled geochemistry of Au and As in pyrite from hydrothermal ore deposits. *Geochimica et Cosmochimica Acta*, 140, 644-670.

Deditius, A.P., Utsunomiya, S., Renock, D., Ewing, R.C., Ramana, C.V., Becker, U., & Kesler, S.E. (2008). A proposed new type of arsenian pyrite: Composition, nanostructure and geological significance. *Geochimica et Cosmochimica Acta*, 72, 2919-2933.

Deer, W.A., Howie, R.A., & Zussman, J. (2013). An introduction to the rock-forming minerals. London: The Mineralogical Society.

de Obeso, J.C., & Kelemen, P.B. (2020). Major element mobility during serpentinization, oxidation and weathering of mantle peridotite at low temperatures. *Phil. Trans. R. Soc. A* 378: 20180433.

Droop, G.T.R. (1987). A general equation for estimating Fe^{3+} concentrations in ferromagnesian silicates and oxides from microprobe analysis, using stoichiometric criteria. *Mineral Magazine*, 51, 431-437.

Fleet, M.E., Liu, X., & King, P.L. (2004). Accommodation of the carbonate ion in apatite: An FTIR and X-ray structure study of crystals synthesized at 2-4 GPa. *American Mineralogist*, 89, 1422-1432.

Forshaw, J.B., & Pattison, D.R.M. (2021). Ferrous/ferric (Fe^{2+}/Fe^{3+}) partitioning among silicates in metapelites. *Contributions to Mineralogy and Petrology*, 176, 1-26.

Franz, G., & Spear, F.S. (1985). Aluminous titanite from the Eclogite Zone, south central Tauern Window, Austria. *Chemical Geology*, 50, 33-46.

Goldoff, B., Webster, J.D., & Harlov, D. (2012). Characterization of fluor-chlorapatites by electron probe microanalysis with a focus on time-dependent intensity variation of halogens. *American Mineralogist*, 97, 1103-1115.

Grew, E.S., Locock, A.J., Mills, S.J., Galuskina, I.O., Galuskin, E.V., & Hålenius, U. (2013). Nomenclature of the garnet supergroup. *American Mineralogist*, 98, 785-811.

Hammerli, J., Hermann, J., Tollan, P., & Naab, F. (2021). Measuring in situ CO2 and H2O in apatite via ATR-FTIR. *Contributions to Mineralogy and Petrology*, 176, 105.

Hawthorne, F.C., Oberti, R., Harlow, G.E., Maresch, W.V., Martin, R.F., Schumacher, J.C., & Welch, M.D. (2012). Nomenclature of the amphibole supergroup. *American Mineralogist*, 97, 2031-2048.

Hawthorne, F.C., Ungaretti, L., Oberti, R., Caucia, F., & Callegari, A. (1993). The crystal chemistry of staurolite. I. Crystal structure and site populations. *The Canadian Mineralogist*, 31, 551-582.

Harlow, G.E. (1999). Interpretation of Kcpx and CaEs components in clinopyroxene from diamond inclusions and mantle samples. Proceedings of the 7th *International Kimberlite Conference*, 1, 321-331.

Hey, M.H. (1954). A new review of the chlorites. *Mineralogical Magazine*, 30, 277-292.

Holdaway, M.J., Mukhopadhyay, B., Dyar, M.D., Dutrow, B.L., Rumble, D., & Grambling, J.A. (1991). A new perspective on staurolite crystals chemistry: Use of stoichiometric and chemical end-members for a mole fraction model. *American Mineralogist*, 76, 1910-1991.

Ketcham, R.A. (2015). Technical Note: Calculation of stoichiometry from EMP data for apatite and other phases with mixing on monovalent anion sites. *American Mineralogist*, 100, 1620-1623.

Kohn, M.J. (2017). Titanite petrochronology. *Reviews in Mineralogy and Geochemistry*, 83, 419-441.

Leake, B.E., Woolley, A.R., Arps, C.E.S., Birch, W.D., Gilbert, M.C., Grice, J.D., Hawthorne, F.C., Kato, A., Kish, H.J., Krivovichev, V.G., Linthout, K., Laird, J., Mandarino, J.A., Maresch, W.V., Nickel, E.H., Rock, N.M.S., Schumacher, J.C., Smith, D.C., Stephenson, N.C.N., Ungaretti, L., Whittaker, E.J.W., & Youzhi, G. (1997). Nomenclature of amphiboles: Report of the subcommittee on amphiboles of the International Mineralogical Association, Commission on New Minerals and Mineral Names. *The Canadian Mineralogist*, 35, 219-246.

Li, X., Zhang, C., Behrens, H., & Holtz, F. (2020). Calculating biotite formula from electron microprobe analysis data using a machine learning method based on principal components regression. Lithos, 356-357: 105371.

Le Pioufle, A., & Canil, D. (2012). Iron in monticellite as an oxygen barometer for kimberlite magmas. *Contributions to Mineralogy and Petrology*, 163, 1033-1046.

Lockock, A.J. (2014). An Excel spreadsheet to classify chemical analyses of amphibole following the IMA 2012 recommendations. *Computers & Geosciences*, 62, 1-14.

Masci, L., Dubacq, B., Verlaguet, A., Chopin, C., de Andrade, V., & Herviou, C. (2019). A XANES and EPMA study of Fe^{3+} in chlorite: Importance of oxychlorite and implications for cation site distribution and thermobarometry. *American Mineralogist*, 104, 403-417.

Morimoto, N., Fabries, J., Fergusson, A.K., Ginzburg, I.V., Ross, M., Seifert, F.A., Zussman, J., Aoki, K., & Gottardi, G. (1989). Nomenclature of pyroxenes. *Mineralogical Journal*, 14, 198-221.

Oberti, R., Ungretti, L., Cannnillo, E., & Hawthorne, F.C. (1992). The behaviour of Ti in amphiboles. I. Four- and six-coordinate Ti in richterite. *European Journal of Mineralogy*, 4, 425-439.

Piccardo, G.B., & Guarnieri, L. (2011). Gabbro-norite cumulates from strongly depleted MORB melts in the Alpine-Apennine ophiolites. *Lithos*, 124, 200-214.

Qian, G., Brugger, J., Testemale, D., Skinner, W., & Pring, A. (2013). Formation of As(II)-pyrite during experimental replacement of magnetite under hydrothermal conditions. *Geochimica et Cosmochimica Acta*, 100, 1-10.

Sadove, G., Konecke, B.A., Fiege, A., & Simon, A.C. (2019). Structurally bound S^{2-}, S^{1-}, S^{4+}, S^{6+} in terrestrial apatite: The redox evolution of hydrothermal fluids at the Phillips mine, New York, USA. *Ore Geology Reviews*, 107, 1084-1096.

Schumacher, J.C. (1991). Empirical ferric iron corrections: Necessity, assumptions, and effects on selected geothermobarometers. *Mineralogical Magazine*, 55, 3-18.

Sorcar, N., Joshi, K.B., Olivera, E.P., Tomson, J.K., & Nandakumar, V. (2020). Characterization of partial melting events in garnet-cordierite gneiss from the Kerala Khondalite Belt, India. *Geoscience Frontiers*, 11 (2), 587-611.

Stumpf, S., Skrzypek, E., & Stüwe, K (2024). Dating prograde metamorphism: U–Pb geochronology of allanite and REE-rich epidote in the Eastern Alps. *Contributions to Mineralogy and Petrology*, 179 (63), 1-24.

Tiepolo, M., Zanetti, A., & Oberti, R. (1999). Detection, crystal-chemical mechanisms and petrological implications of $^{[6]}Ti^{4+}$ partitioning in pargasite and kaersutite. *European Journal of Mineralogy*, 11, 345-354.

Tropper, P., Wyhlidal, S., Haefeker, U.A., & Mirwald, P.W. (2018). An experimental investigation of Na incorporation in cordierite in low P/high T metapelites. *Mineralogy and Petrology*, 112, 199-217.

Walters, J.B., & Kohn, M.J. (2017). Protracted thrusting followed by late rapid cooling of the Greater Himalayan Sequence, Annapurna Himalaya, Central Nepal: Insights from titanite petrochronology. *Journal of Metamorphic Geology*, 35, 897-917.

Walters, J.B., Cruz-Uribe, A.M., & Marschall, H.R. (2019). Isotopic compositions of sulfides in exhumed high-pressure terranes: Implications for sulfur cycling in subduction zones. *Geochemistry, Geophysics, Geosystems*, 20, 2019GC008374.

Walters, J.B., Cruz-Uribe, A.M., Marschall, H.R., & Boucher, B. (2021). The role of sulfides in the chalcophile and siderophile element budget of the subducted oceanic crust. *Geochimica et Cosmochimica Acta*, 304, 191-215.

Walters, J.B., Cruz-Uribe, A.M., Song, W.J., Gerbi, C., & Biela, K. (2022). Strengths and limitations of in situ U-Pb titanite petrochronology in polymetamorphic rocks: An example from western Maine, USA. *Journal of Metamorphic Geology*, 40, 1043-1066.

Walters, J.B. (2022). MinPlot: A mineral formula recalculation and plotting program for electron probe microanalysis. *Mineralogia*, 53 (1), 51-66.

Warr, L.N. (2021). IMA-CNMNC approved mineral symbols. *Mineralogical Magazine*, 85, 291-320.

Wiewióra, A., & Weiss, Z. (1990). Crystallochemical classifications of phyllosilicates based on the unified system of projection of chemical composition: II. The chlorite group. *Clay Mineralogy*, 25, 83–92.

Wolfsdorff, P., & Schreyer, W. (1992) Synthesis of sodian cordierites in the system Na_2O-MgO-Al_2O_3-SiO_2. *Neues Jb Miner Monat*, 2, 80–96.

Jesse B. Walters & Nils B. Gies
15.12.2024